Supporting Information

Dynamic selection in metallo-organic cube $Cd^{II}_8L_4$ conformations induced by perfluorooctanoate encapsulation

Yu-Qing Li,[a,#] He Zhao,[a,#] Er-Meng Han,[a] Zhiyuan Jiang,[c,*] Qixia Bai,[b] Yu-Ming Guan,[b] Zhe Zhang,[b] Tun Wu,[b,*] Pingshan Wang[a,*]

Table of Contents

1. General Procedures

All starting materials were purchased from Aldrich and Alfa Aesar, and used without further purification. Compound **1** and **3** were synthesized according to the reported methods[S1, S2]. Column chromatography was conducted using basic Al_2O_3 (Sinopharm Chemical Reagents Co. Ltd, 200-300 mesh) or SiO_2 (Qingdao Haiyang Chemical Co., Ltd, 200-300 mesh) and the separated products were confirmed by NMR spectra using a Bruker Avance 400-MHz or 500-MHz NMR spectrometers in $CDCl_3$, and, CD_3CN with a TMS standard. Electro-spray ionization (ESI) mass spectra were recorded with a Bruker microOTOF-QII or a Waters Synapt HDMS G2 instrument, using solutions of 0.01 mg/mL in $CHCl_3$/MeCN (1:3, v/v) for ligands and 0.2 mg/mL in MeCN or MeCN/MeOH (3:1, v/v) for complexes.

NMR. Nuclear magnetic resonance spectra data were recorded on a Bruker 500 MHz, a Bruker 500 MHz and a 400 MHz nuclear magnetic resonance instrument using, $CDCl_3$ and CD_3CN as the solvents with tetramethylsilane (TMS) as the internal standard at 25 °C.

ESI-MS and **TWIM-MS.** ESI mass spectrometry and traveling wave ion mobility (TWIM) experiments were conducted on a Waters Synapt HDMS G2 instrument with a LockSpray ESI source, using the following parameters: ESI capillary voltage, 1.3-3.0 kV; sample cone voltage, 20-25 V; extraction cone voltage, 1.1-3 V; desolvation gas flow, 800 L/h (N_2); trap collision energy (CE), 4 V; transfer CE, 0 V; trap gas flow, 2.0 mL/min (Ar); source temperature, 30 °C; and desolvation temperature, 30 °C. All samples were dissolved in CH_3CN or CH_3CN/CH_3OH (1:1, v/v) and then infused into the -100, KD Scientific). For TWIM experiments, the helium cell gas flow was held at 180.0 mL/min and the ion mobility cell gas flow was held at 90.0 mL/min (N_2). The TWIM DC traveling wave velocity and height were set as 683 m/s and 26.3 V, respectively. Data were collected and analyzed by using MassLynx 4.1 and DriftScope 2.4 (Waters).

UV-vis absorption. UV-vis absorption spectra were recorded on a Thermo Fisher Scientific Evolution 201 spectrophotometer at room temperature (10^{-6} M in acetonitrile) and were corrected with the background spectrum of the solvent.

Single crystal X-ray diffraction. Single-crystal X-ray diffraction data for D_2-**2** (CCDC: 2359196) w as collected on a Bruker D8 VENTURE METALJET liquid metal Xray source system (GaKα, λ= 1.3 4138 Å) at low temperatures (100 K), equipped with an Oxford 800 Plus liquid nitrogen vapor coolin g device. Using Olex2,[S4] the structures were solved with the SHELXT [S5] structure solution program u sing Intrinsic Phasing and refined with the SHELXL[S6] refinement package using Least Squares mini misation. The contribution of disordered guest molecules to scattering was removed by the SQUEEZ E[S7] program of PLATON.[S8]

Energy calculation method: First-principles calculations are performed by Forcite at Materials Studio. Simulation is performed using a universal force field. The containment limits for energy, maximum force, and maximum displacement are set to $2*10^{-5}$ kcal/mol, 0.001 kcal/mol/Å, e^{-5} Å, respectively. The effects of the counterions were omitted in the modeling. Structures were constructed on the basis of the crystal structures. Valence energy (diag. terms) contains the contributions of bond, angle, torsion, and inversion. Valence energy (cross terms) contains the contributions of stretch-stretch, stretch-bend-stretch, stretch-torsion-stretch, separated-stretch-stretch, torsion-stretch, bend-bend, torsion-bend-bend and bend-torsion-bend. Non-bond energy contains the contributions of van der Waals and electrostatic interactions. All of the energies are reported in kcal/mol.[S9-S10]

2. Synthesis of the Ligands L and metallo-organic cages $Cd^{II}_8L_4$.

Compound **1** were synthesized according to the reported methods[S1].

Compound **3** were synthesized according to the reported methods[S2].

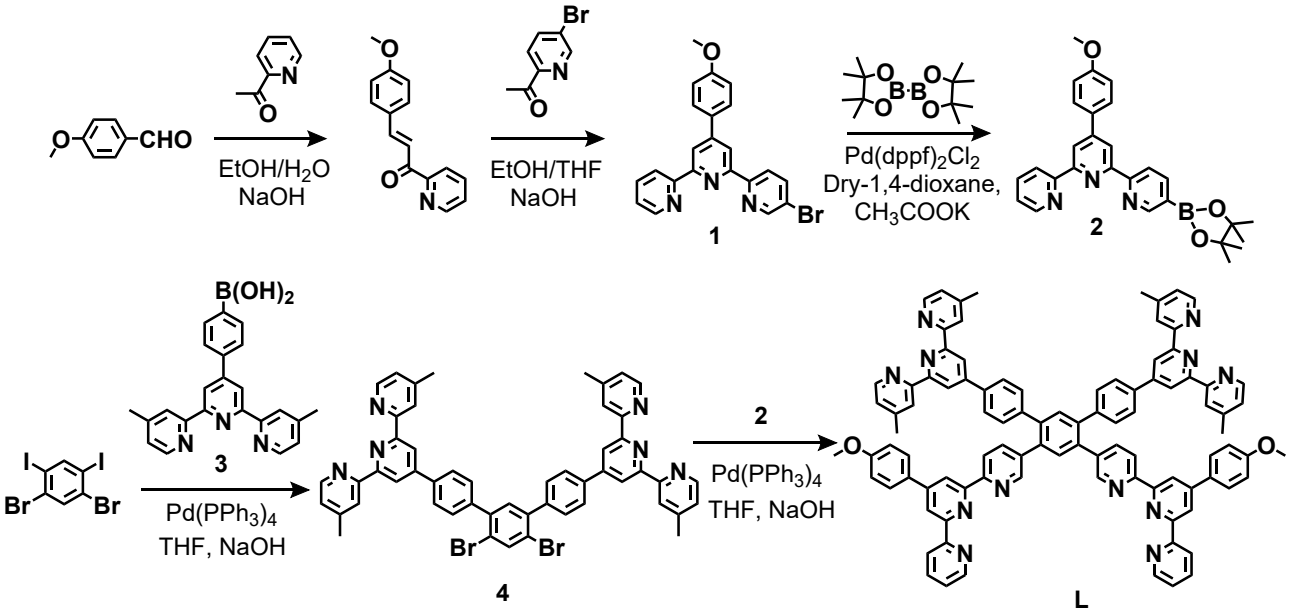

Scheme S1: The synthetic route of ligand **L**.

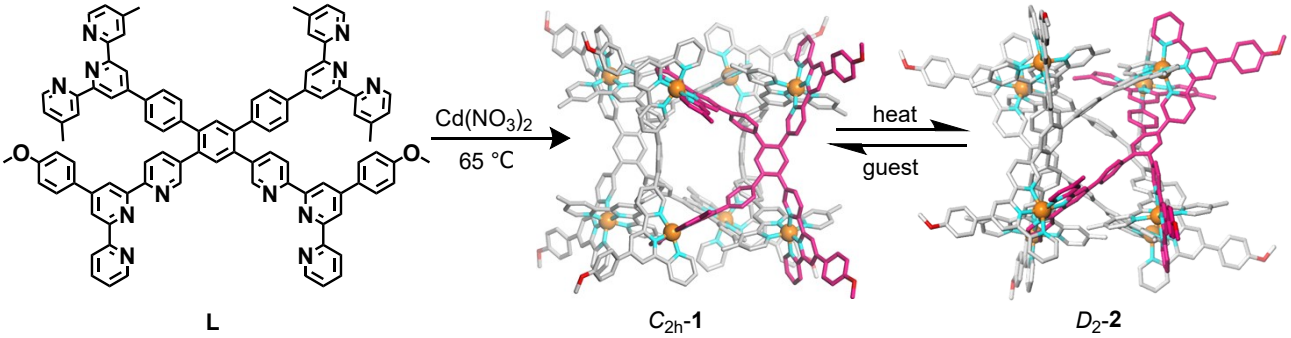

Scheme S2: The synthetic route of metallo-organic cages $Cd^{II}_8L_4$ (*C*$_{2h}$-**1** and *D*$_2$-**2**).

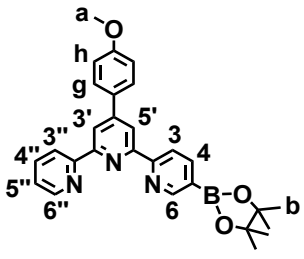

Compound 2: Mixing compound **1** (1.3 g, 3.0 mmol) and Bis(pinacolato)diboron (0.9 g, 3.6 mmol) into a 100 mL flask, then 1,4-Dioxane (50 mL), and CH_3COOK (0.9 g, 9.0 mmol) was added. The system was degassed for 10 min, and $Pd(dppf)_2Cl_2$ (150 mg, 0.2 mmol) as the catalyst was added. The mixture was stirred at 85 °C under nitrogen for 8 h, after cooled to ambient temperature. Concentrated

in vacuo followed by adding CH_2Cl_2 to dissolve the product, filtered, then removed CH_2Cl_2 under vacuum to give the product, as white solid: 1.3 g, 93%. ^{1}H NMR (400 MHz, $CDCl_3$) δ 8.98 (s, 1H, tpy-$H^{3'}$), 8.69 (s, 1H, tpy-$H^{5'}$), 8.69-8.64 (m, 2H, tpy-$H^{6,6''}$), 8.62-8.60 (d, 1H, J= 8 Hz, tpy-H^{3}), 8.58-8.56 (d, 1H, J= 8 Hz, tpy-$H^{3''}$), 8.18-8.16 (d, 1H, J= 8 Hz, tpy-H^{4}), 7.84-7.81 (m, 3H, tpy-$H^{4''}$, Ph-H^{g}), 7.30-7.27 (m, 1H, tpy-$H^{5''}$), 6.98-6.96 (d, 2H, J= 8 Hz, Ph-H^{h}), 3.82 (s, 3H, H^{a}), 1.33 (s, 12H, H^{b}). ^{13}C NMR (126 MHz, $CDCl_3$) δ 160.54, 158.29, 156.37, 155.90, 155.83, 155.05, 149.73, 149.08, 143.13, 136.86, 130.76, 128.55, 123.75, 121.42, 120.44, 118.77, 118.53, 114.35, 84.23, 55.37, 24.91. ESI-MS (465.4 calcd. For $C_{28}H_{28}BN_3O_3$): *m/z* 466.231 $[M + H^+]^+$ (calcd *m/z*: 466.231).

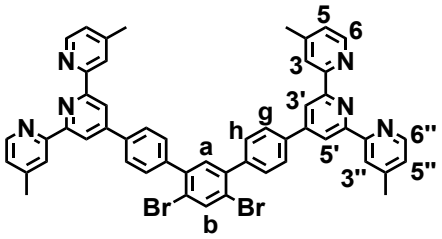

Compound 4: 1,5-dibromo-2,4-diiobenzene (3.0 g, 6.2 mmol) and compound **3** (4.5 g, 12.4 mmol) was added to a 500 mL flask, then THF (200 mL) and NaOH (1.5 g, 37.2 mmol) in 30 mL of water was added. The system was degassed for 10 min, and $Pd(PPh_3)_4$ (346.0 mg, 0.3 mmol) as the catalyst was added. The mixture was stirred at 65 °C under nitrogen for 2 d, after cooled to ambient temperature, then concentrated in vacuo followed by column chromatography (Al_2O_3), eluting with the mixture of petroleum ethe and CH_2Cl_2 (v/v, 1:3) to pure the product, as white solid: 3.0 g, 54%. ^{1}H NMR (400 MHz, $CDCl_3$) δ 8.76 (s, 4H, tpy-$H^{3',5'}$), 8.59-8.58 (d, 4H, J= 4 Hz, tpy-$H^{6,6''}$), 8.47 (s, 4H, tpy-$H^{3,3''}$), 8.05 (s, 1H, H^{b}), 8.00-7.98 (d, 4H, J= 8 Hz, Ph-H^{g}), 7.61-7.59 (d, 4H, J= 8 Hz, Ph-H^{h}), 7.43 (s, 1H, H^{a}), 7.19-7.18 (d, 4H, J= 4 Hz, tpy-$H^{5,5''}$). ^{13}C NMR (101 MHz, $CDCl_3$) δ 156.21, 155.96, 149.54, 149.00, 148.09, 141.33, 140.32, 138.12, 136.89, 133.06, 129.86, 127.15, 124.89, 122.15, 121.96, 119.04, 21.40. ESI-MS (906.7 calcd. For $C_{52}H_{38}Br_2N_6$): *m/z* 907.161 $[M + H^+]^+$ (calcd *m/z*: 907.151).

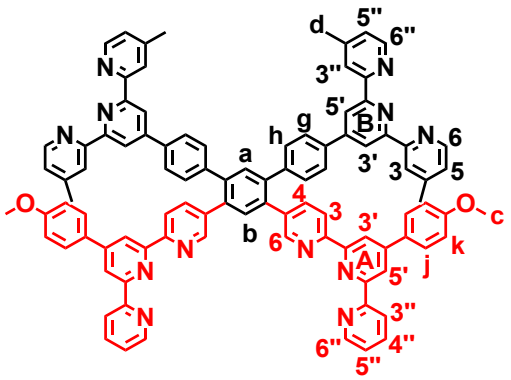

Compound L: To a solution of **4** (1.5 g, 1.7 mmol) and **2** (2.1 g, 4.4 mmol) in 140 mL THF, NaOH

(408 mg, 10.2 mmol) was added. The mixture was degassed for three times and backfilled with Argon, then $Pd(PPh_3)_4$ (230.0 mg, 0.2 mmol) was added. After refluxing for 2 d, the mixture was cooled to 25 °C and poured into CH_2Cl_2 solvent. Collecting organic layers, and then the aqueous layer was extracted by CH_2Cl_2. The combined organic phase was washed with brine and dried with Na_2SO_4. After concentration in vacuo, the residue was purified by flash column chromatography (Al_2O_3 200-300 mesh), eluting with CH_2Cl_2: CH_3OH (v/v, 100/0.25) to give **L**, as a white solid: 1.7 g (73%). ^{1}H NMR (600 MHz, $CDCl_3$) δ 8.75-8.74 (d, 2H, *J*= 6 Hz, A-tpy-*H*$^{3'}$), 8.73-8.72 (m, 6H, A-tpy-*H*$^{5'}$, B-tpy-*H*$^{3',5'}$), 8.70-8.69 (m, 4H, A-tpy-*H*^{3}, A-tpy-*H*^{6}), 8.68-8.67 (d, 2H, *J*= 6 Hz, A-tpy-*H*$^{3''}$), 8.64-8.63 (d, 2H, *J*= 6 Hz, A-tpy-*H*$^{6''}$), 8.55-8.54 (d, 4H, *J*= 6 Hz, B-tpy-*H*$^{6,6''}$), 8.45 (s, 4H, B-tpy-*H*$^{3,3''}$), 7.90-7.89 (d, 4H, *J*= 6 Hz, A-Ph-*H*^{j}), 7.88-7.87 (d, 4H, *J*= 6 Hz, B-Ph-*H*^{g}), 7.84-7.81 (t, 2H, *J*= 9 Hz, A-tpy-*H*$^{4''}$), 7.79 (s, 1H, *H*^{a}), 7.77-7.76 (d, 2H, *J*= 6 Hz, A-tpy-*H*^{4}), 7.75 (s, 1H, *H*^{b}), 7.50-7.48 (d, 4H, *J*= 12 Hz, B-Ph-*H*^{h}), 7.32-7.30 (t, 2H, *J*= 6 Hz, A-tpy-*H*$^{5''}$), 7.16-7.15 (d, 4H, *J*= 6 Hz, B-tpy-*H*$^{5,5''}$), 7.01-6.99 (d, 4H, *J*= 12 Hz, A-Ph-*H*^{j}), 3.86 (s, 6H, *H*^{c}), 2.50 (s, 12H, *H*^{d}). ^{13}C NMR (151 MHz, $CDCl_3$) δ 160.44, 156.39, 156.21, 156.01, 155.82, 155.43, 154.87, 149.74, 149.63, 149.53, 148.99, 148.03, 140.79, 140.48, 138.00, 137.41, 136.87, 136.72, 136.26, 130.81, 130.51, 128.57, 127.50, 124.83, 123.71, 122.10, 121.53, 120.71, 118.96, 118.45, 118.27, 114.27, 21.37. ESI-MS (1423.7 calcd. For $C_{96}H_{70}N_{12}O_2$): *m/z* 1425.501 $[M + H^+]^+$ (calcd *m/z*: 1425.501).

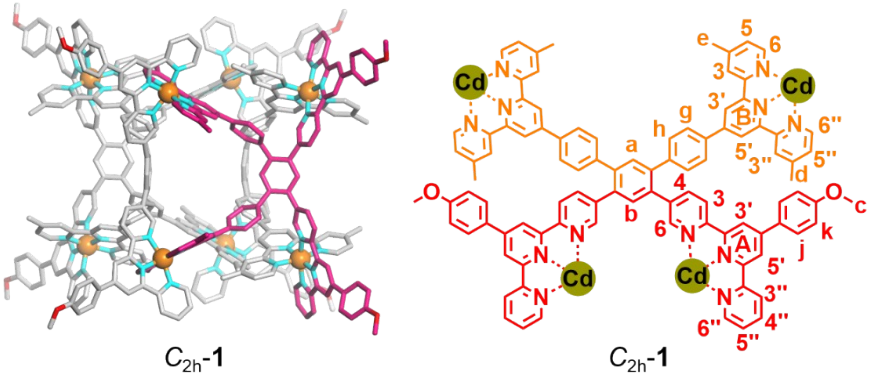

C_{2h}-**1** C_{2h}-**1**

Cube-shaped supermolecule C_{2h}-1: Ligand **L** (30.0 mg, 21.1 μmol), and $Cd(NO_3)_2$ (13.1 mg, 42.2 μmol) was added in a 100 mL flask, then a solvent mixture of $CHCl_3$/MeOH (45 mL, v/v, 3/4) was added. The mixture was refluxed for 12 h, after cooled to ambient temperature, excess $LiNTf_2$ in MeOH was added to get a white precipitate, which was filtered and washed with H_2O and MeOH to generate a white solid: 60.1 mg (96%). ^{1}H NMR (400 MHz, CD_3CN) δ 9.49 (s, 8H, B-tpy-*H*$^{3'}$), 9.32 (s, 8H, B-tpy-*H*^{3}), 8.92-8.90 (m, 16H, A-tpy-*H*$^{3'}$, A-tpy-*H*$^{3''}$), 8.68 (s, 8H, A-tpy-*H*$^{5'}$), 8.57-8.56 (d, 8H, *J*= 4 Hz, A-tpy-*H*$^{6''}$), 8.43-8.36 (m, 24H, A-tpy-*H*$^{4''}$, A-tpy-*H*^{3}, B-tpy-*H*$^{5'}$), 8.25-8.22 (m, 24H, B-tpy-*H*$^{3''}$, B-Ph-*H*^{g}), 8.10-8.08 (d, 16H, *J*= 8 Hz, A-Ph-*H*^{j}), 7.95-7.93 (d, 8H, *J*= 12 Hz, A-tpy-*H*^{4}), 7.86-7.85 (d, 8H, *J*= 4 Hz, B-tpy-*H*^{6}), 7.82-7.81 (d, 8H, *J*= 4 Hz, B-tpy-*H*$^{6''}$), 7.76-7.73 (t, 6H, A-tpy-*H*$^{5''}$),

7.27-7.25 (d, 8H, *J*= 8 Hz, B-tpy-H^5), 7.23-7.21 (d, 16H, *J*= 4 Hz, A-Ph-H^k), 7.08-7.06 (d, 16H, *J*= 8 Hz, B-Ph-H^h), 7.04-7.03 (d, 8H, *J*= 4 Hz, B-tpy-$H^{5''}$), 6.99 (s, 4H, H^a), 6.85 (s, 4H, H^b), 5.93 (s, 8H, A-tpy-H^6), 5.93 (s, 24H, H^c), 2.45 (s, 24H, H^e), 2.42 (s, 24H, H^d). ESI-MS (10640.0 calcd. For $C_{412}H_{280}Cd_8F_{84}N_{64}O_{70}S_{28}$): *m/z* 827.413 [M – $10NTf_2^-$]$^{10+}$ (calcd *m/z*: 827.413), 950.667 [M – $9NTf_2^-$]$^{9+}$ (calcd *m/z*: 950.667), 1104.362 [M – $8NTf_2^-$]$^{8+}$ (calcd *m/z*: 1104.362), 1302.253 [M – $7NTf_2^-$]$^{7+}$ (calcd *m/z*: 1302.253).

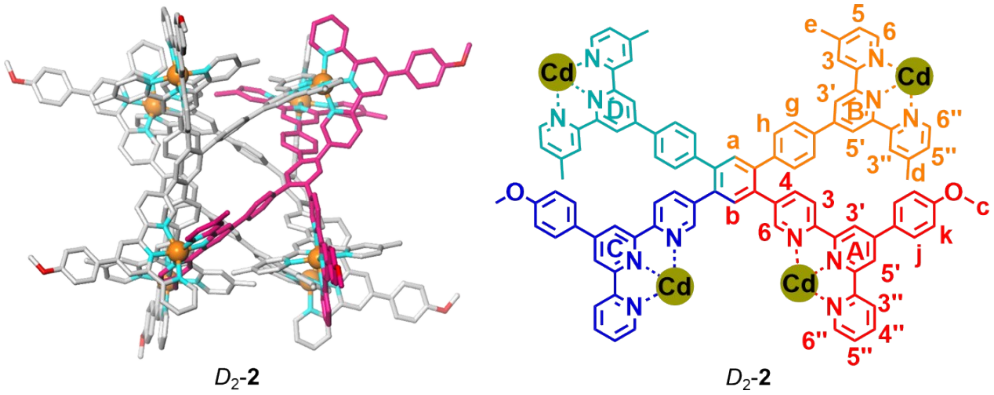

D_2-**2** D_2-**2**

Helical supermolecule D_2-2: Weight 2 mg C_{2h}-**1** and dissolve it in a nuclear magnetic tube with deuterated acetonitrile, heated at 65 °C, and the first day was measured every 3 hours for nuclear magnetic resonance, and the data showed that there was no obvious change. Then the test was carried out at an interval of one day, and there was still no change after a week. So, the test was carried out at an interval of one week. After that a significant change was observed during the test in the third week, and it was changed to a daily test. Finally, all the transformations were detected in the fourth week, and there will be no changes in the following days. ^{1}H NMR (500 MHz, CD_3CN) δ 9.12 (s, 4H, C-tpy-$H^{5'}$), 9.01-8.99 (m, 8H, A-tpy-$H^{5'}$, D-tpy-$H^{5'}$), 8.97-8.95 (m, 8H, C-tpy-$H^{3'}$, D-tpy-$H^{3'}$), 8.82 (m, 8H, A-tpy-$H^{3''}$, C-tpy-$H^{3''}$), 8.73 (m, 8H, B-tpy-$H^{3'}$, B-tpy-$H^{5'}$), 8.71-8.68 (d, 4H, *J*= 15 Hz, C-tpy-H^3), 8.66 (s, 4H, A-tpy-$H^{3'}$), 8.56 (m, 8H, B-tpy-H^3, B-tpy-$H^{3''}$), 8.49 (m, 4H, A-tpy-H^3), 8.44 (m, 8H, D-tpy-H^3, D-tpy-$H^{3''}$), 8.29-8.28 (m, 12H, C-tpy-H^4, C-Ph-H^j), 8.20 (s, 4H, H^a), 8.17-8.16 (m, 16H, A-tpy-$H^{6''}$, C-tpy-$H^{6''}$, A-Ph-H^j), 8.09-8.08 (d, 8H, *J*= 5 Hz, B-tpy-H^6, B-tpy-$H^{6''}$), 7.88-7.82 (m, 20H, A-tpy-$H^{4''}$, B-Ph-H^g, D-Ph-H^g), 7.77-7.75 (m, 8H, A-tpy-H^4, C-tpy-$H^{4''}$), 7.69 (s, 4H, H^b), 7.54-7.53 (m, 4H, C-tpy-H^6), 7.50-7.48 (m, 8H, D-tpy-H^6, D-tpy-$H^{6''}$), 7.33-7.27 (m, 32H, A-tpy-$H^{5''}$, C-tpy-$H^{5''}$, B-Ph-H^h, C-Ph-H^k, D-Ph-H^h), 7.12-7.11 (m, 8H, D-tpy-H^5, D-tpy-$H^{5''}$), 7.06 (m, 4H, A-Ph-H^k), 6.93-6.92 (d, 8H, *J*= 5 Hz, B-tpy-H^5, B-tpy-$H^{5''}$), 5.80 (s, 4H, A-tpy-H^6), 3.99 (s, 12H, C-H^c), 3.94 (s, 12H, A-H^c). ESI-MS (11076.2 calcd. For $C_{416}H_{280}Cd_8F_{96}N_{64}O_{72}S_{32}$): *m/z* 827.414 [M – $10NTf_2^-$]$^{10+}$ (calcd *m/z*: 827.414), 950.657 [M – $9NTf_2^-$]$^{9+}$ (calcd *m/z*: 950.657), 1104.361 [M – $8NTf_2^-$]$^{8+}$ (calcd *m/z*: 1104.361, 1302.249 [M – $7NTf_2^-$]$^{7+}$ (calcd *m/z*: 1302.249).

3. NMR and MS spectra data of Compound and supramolecule.

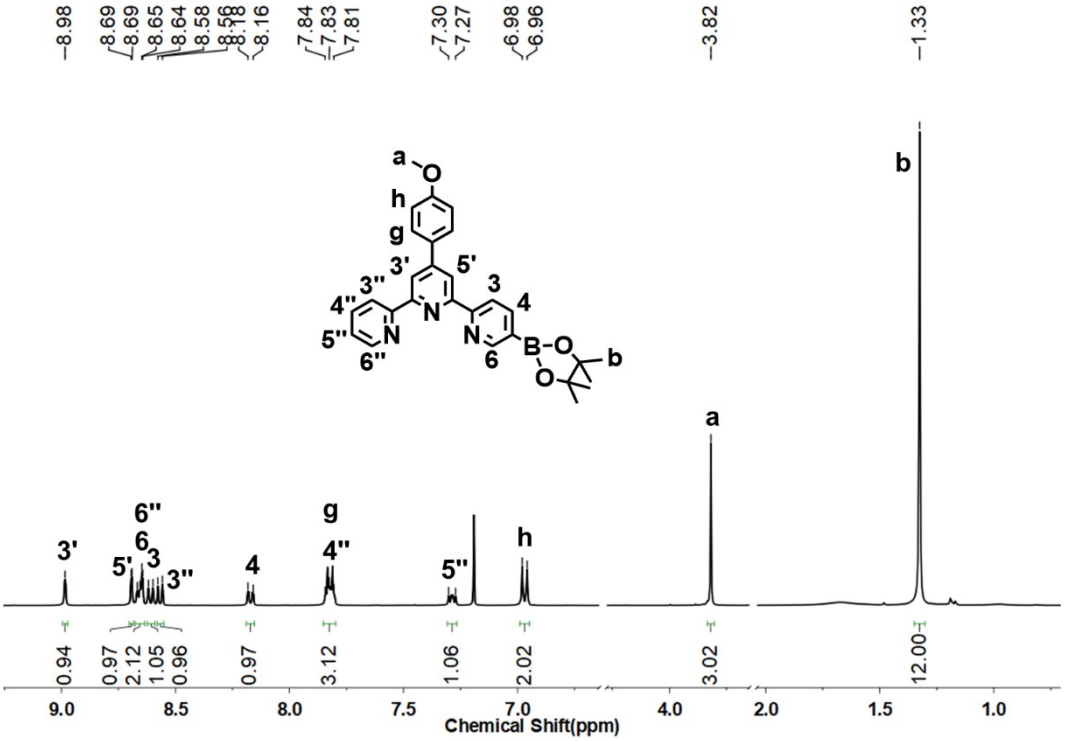

Figure S1: ^{1}H NMR spectrum (400 MHz, 298 K) of **2** in $CDCl_3$.

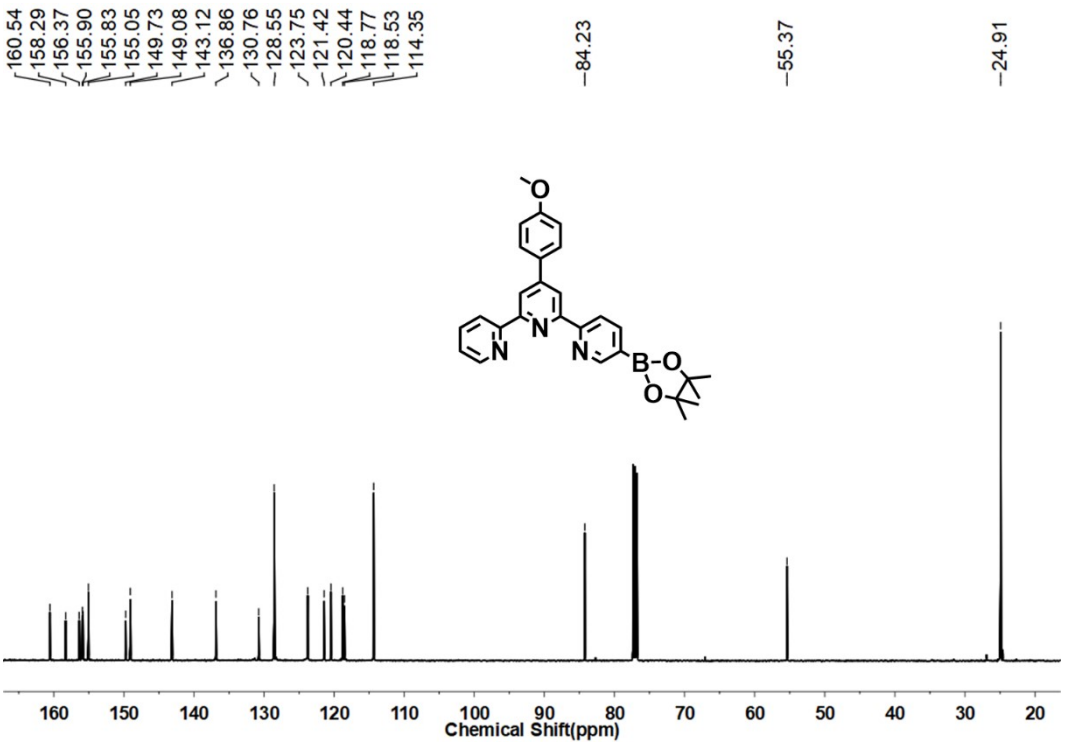

Figure S2: ^{13}C NMR spectrum (126 MHz, 298 K) of **2** in $CDCl_3$.

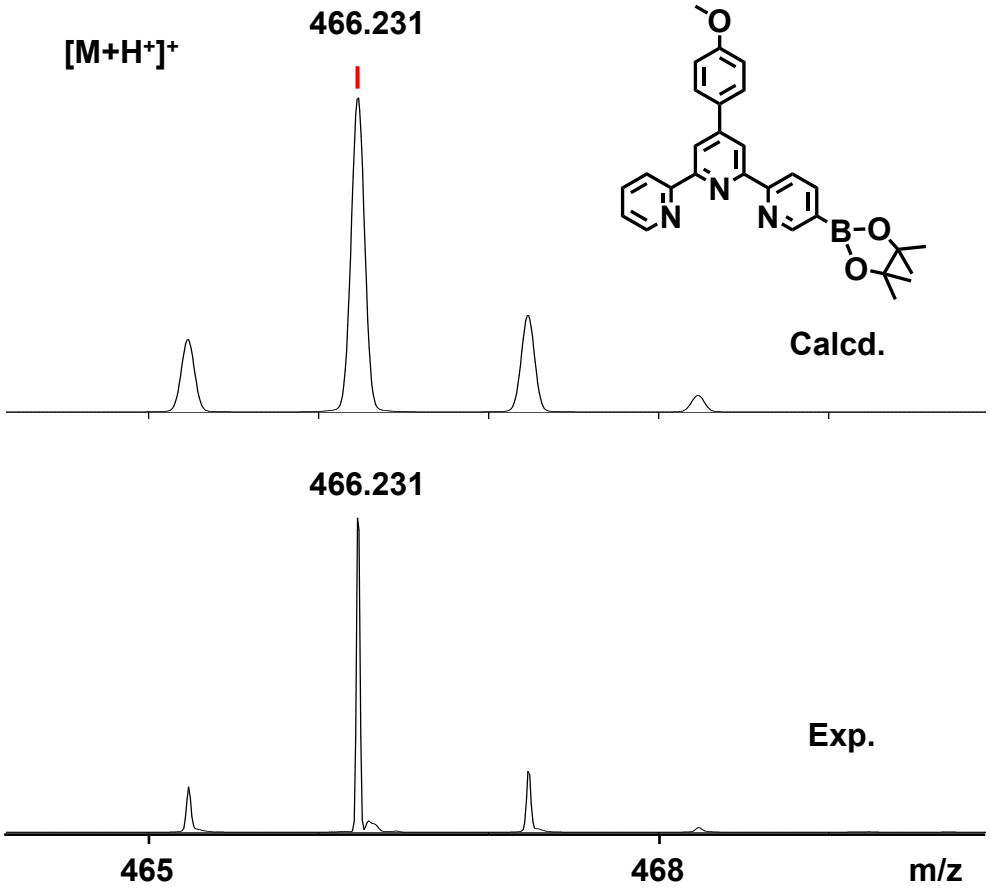

Figure S3: Isotope patterns spectrum of **2**.

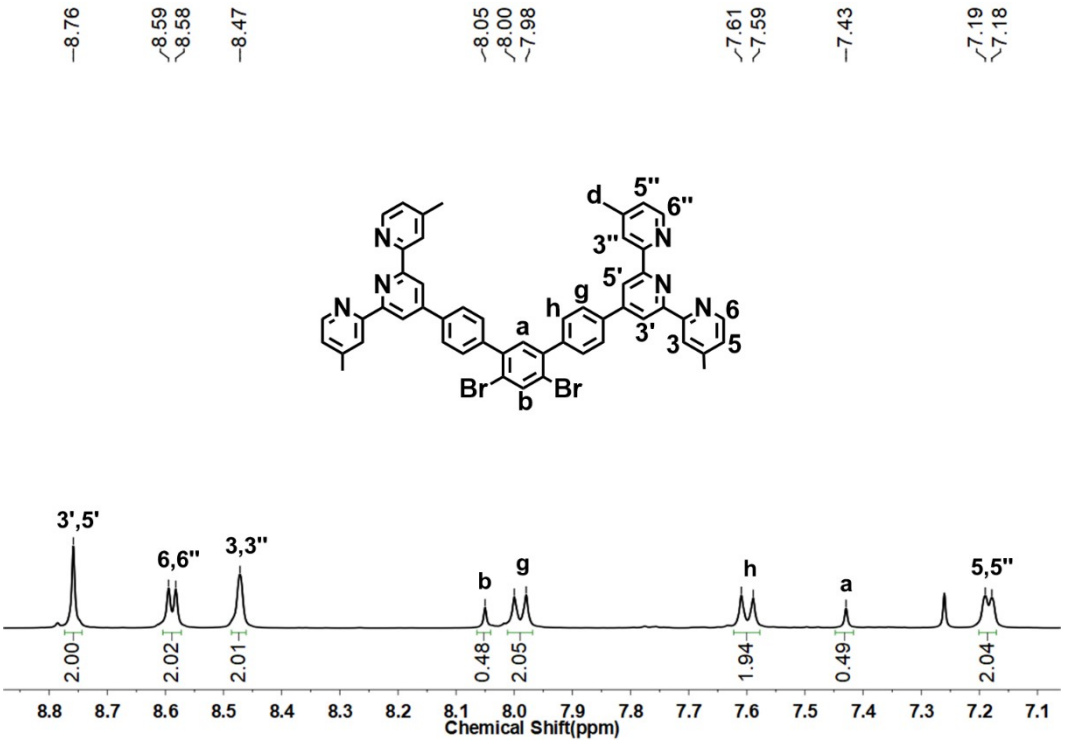

Figure S4: ^{1}H NMR spectrum (400 MHz, 298 K) of **4** in $CDCl_3$.

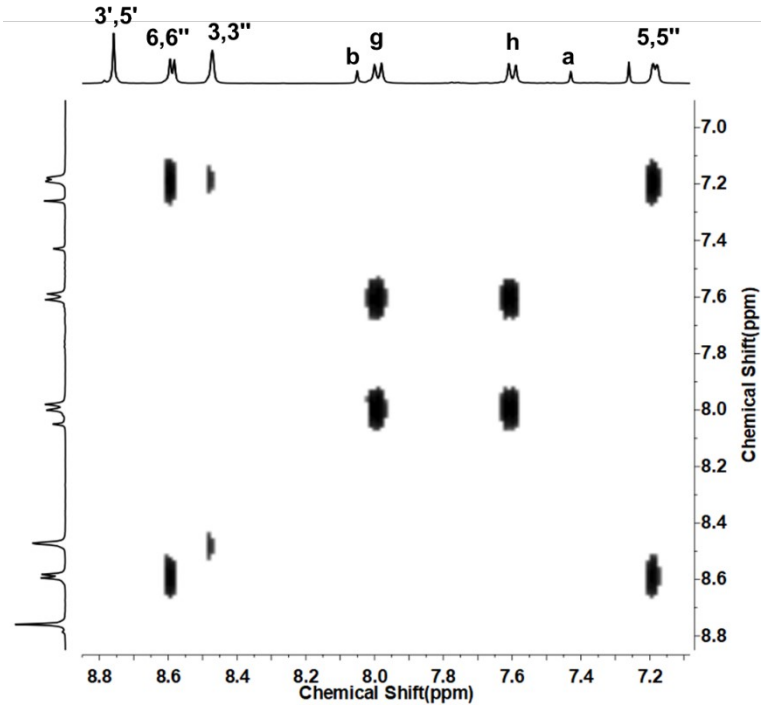

Figure S5: 2D COSY spectrum (400 MHz, 298 K) of **4** in $CDCl_3$.

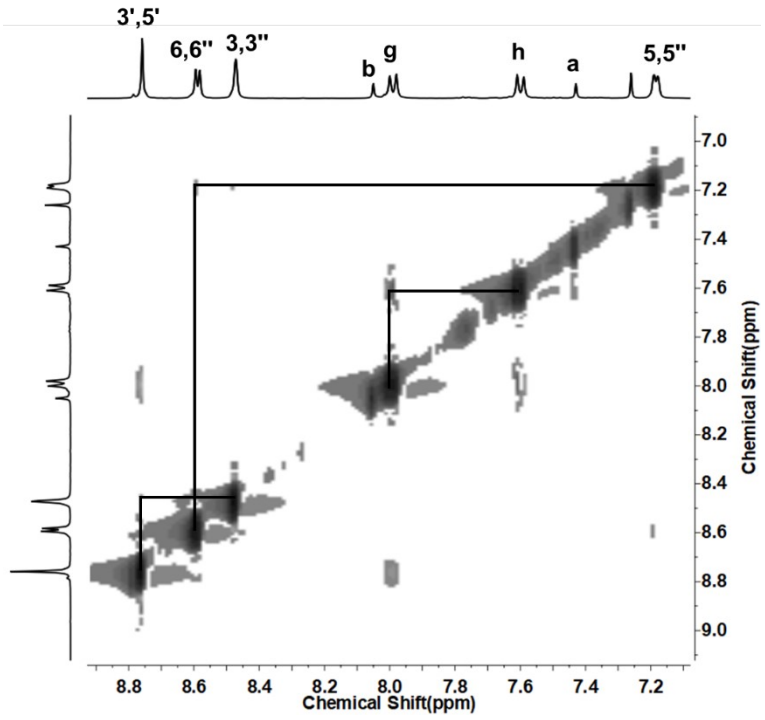

Figure S6: 2D NOESY spectrum (400 MHz, 298 K) of **4** in $CDCl_3$.

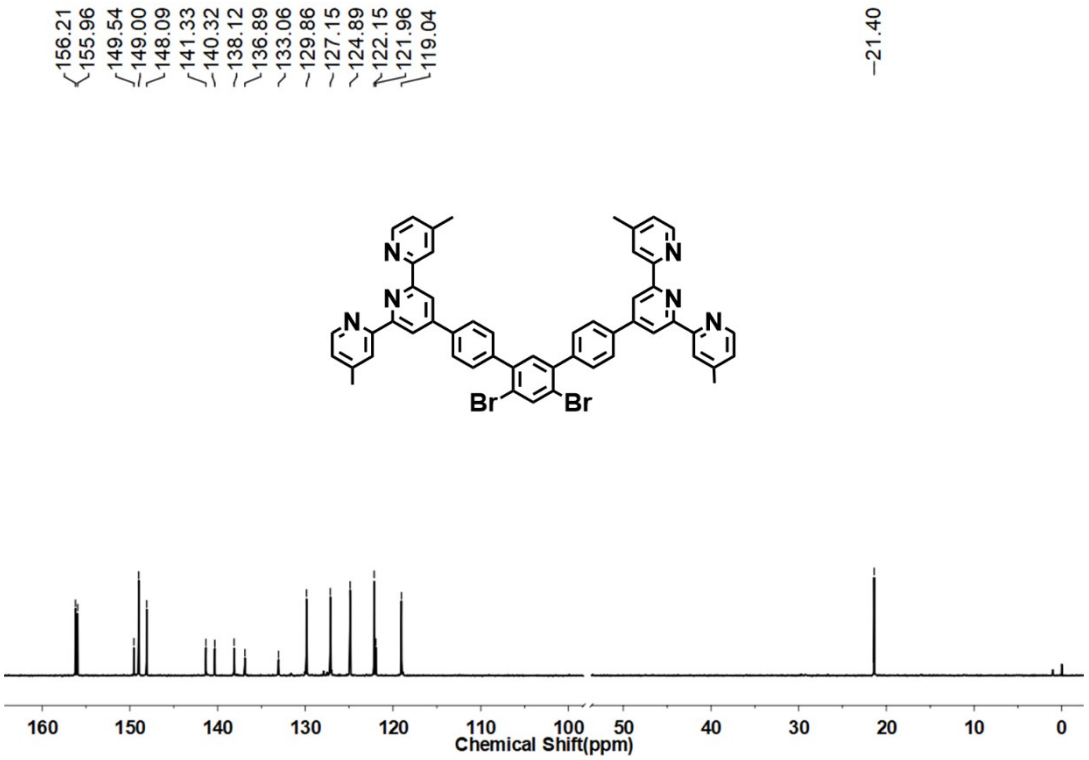

Figure S7: ^{13}C NMR spectrum (101 MHz, 298 K) of **4** in $CDCl_3$.

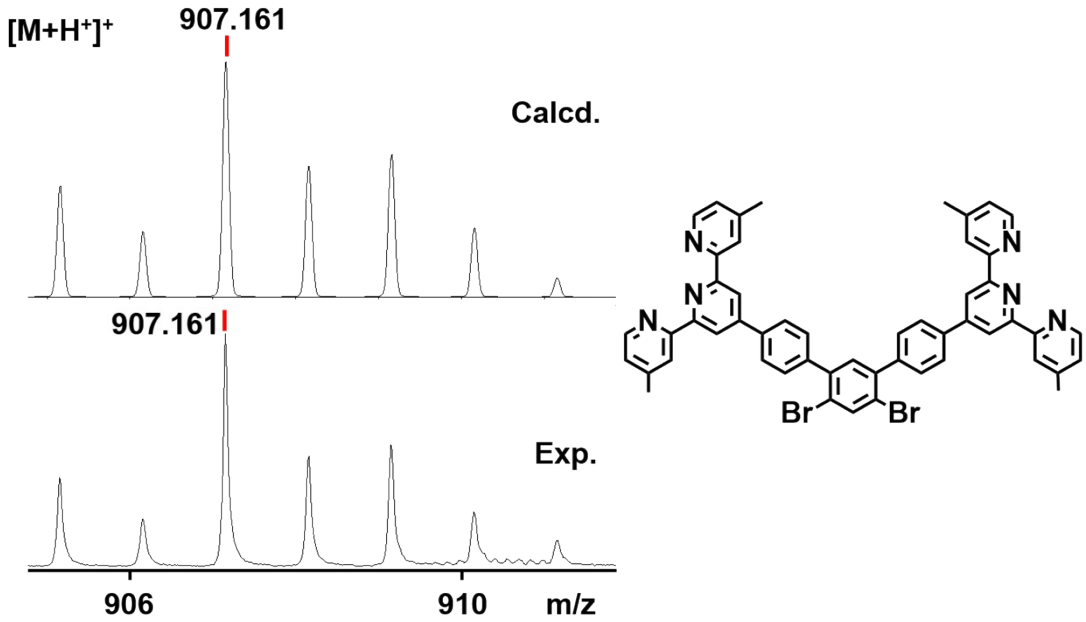

Figure S8: Isotope patterns spectrum of **4**.

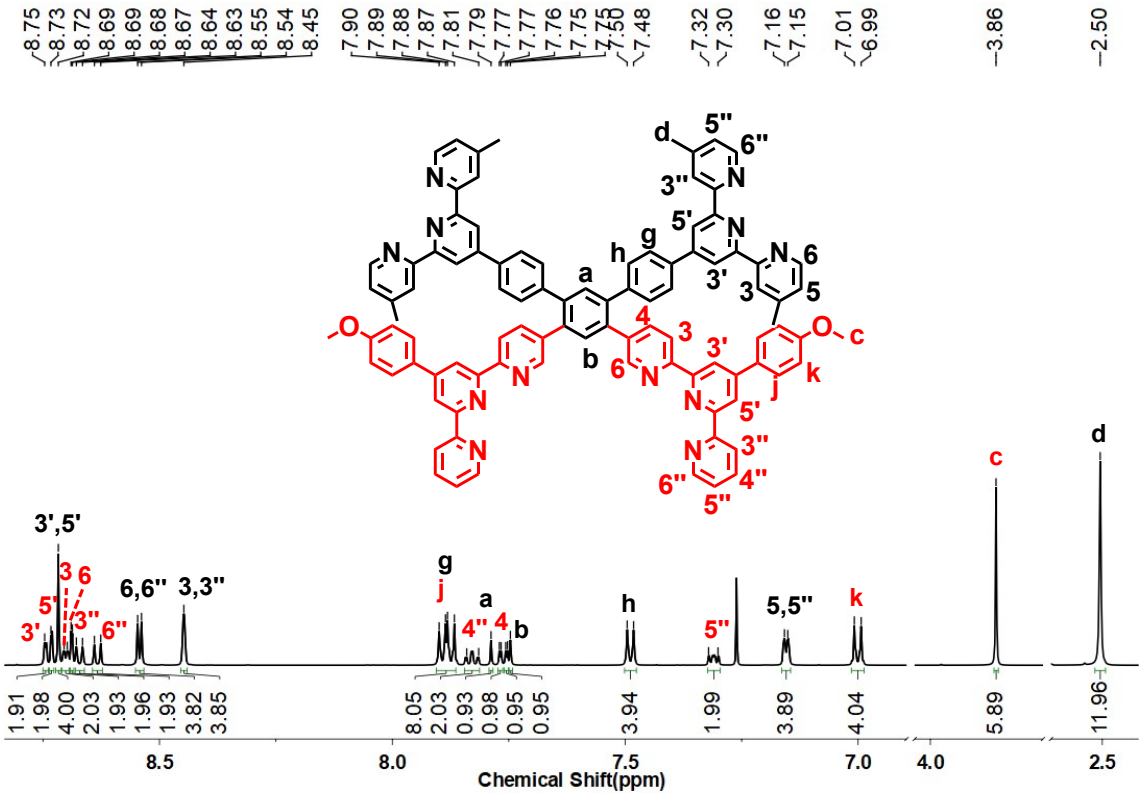

Figure S9: ^{1}H NMR spectrum (600 MHz, 298 K) of **L** in $CDCl_3$.

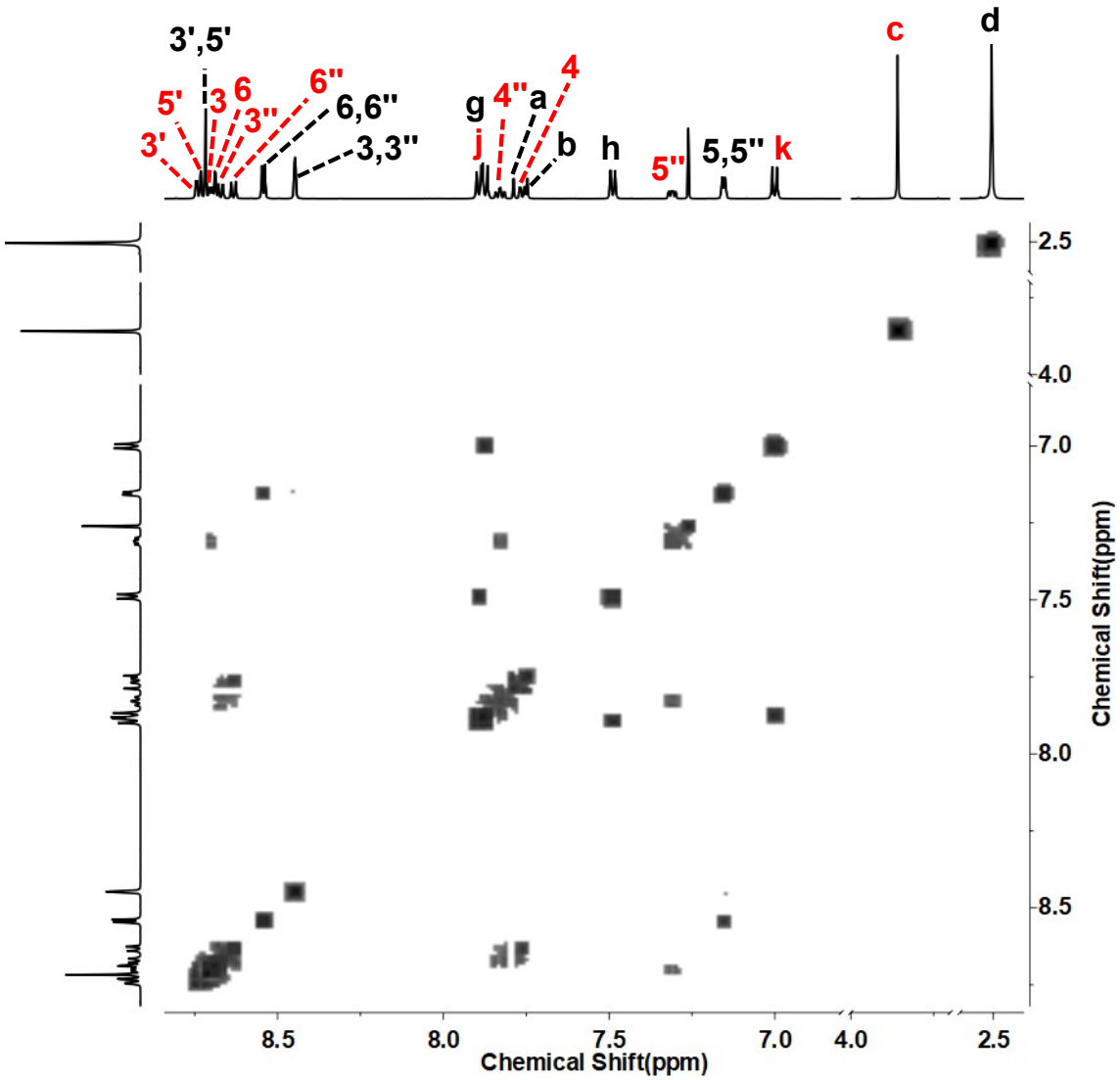

Figure S10: 2D COSY spectrum (600 MHz, 298 K) of **L** in $CDCl_3$.

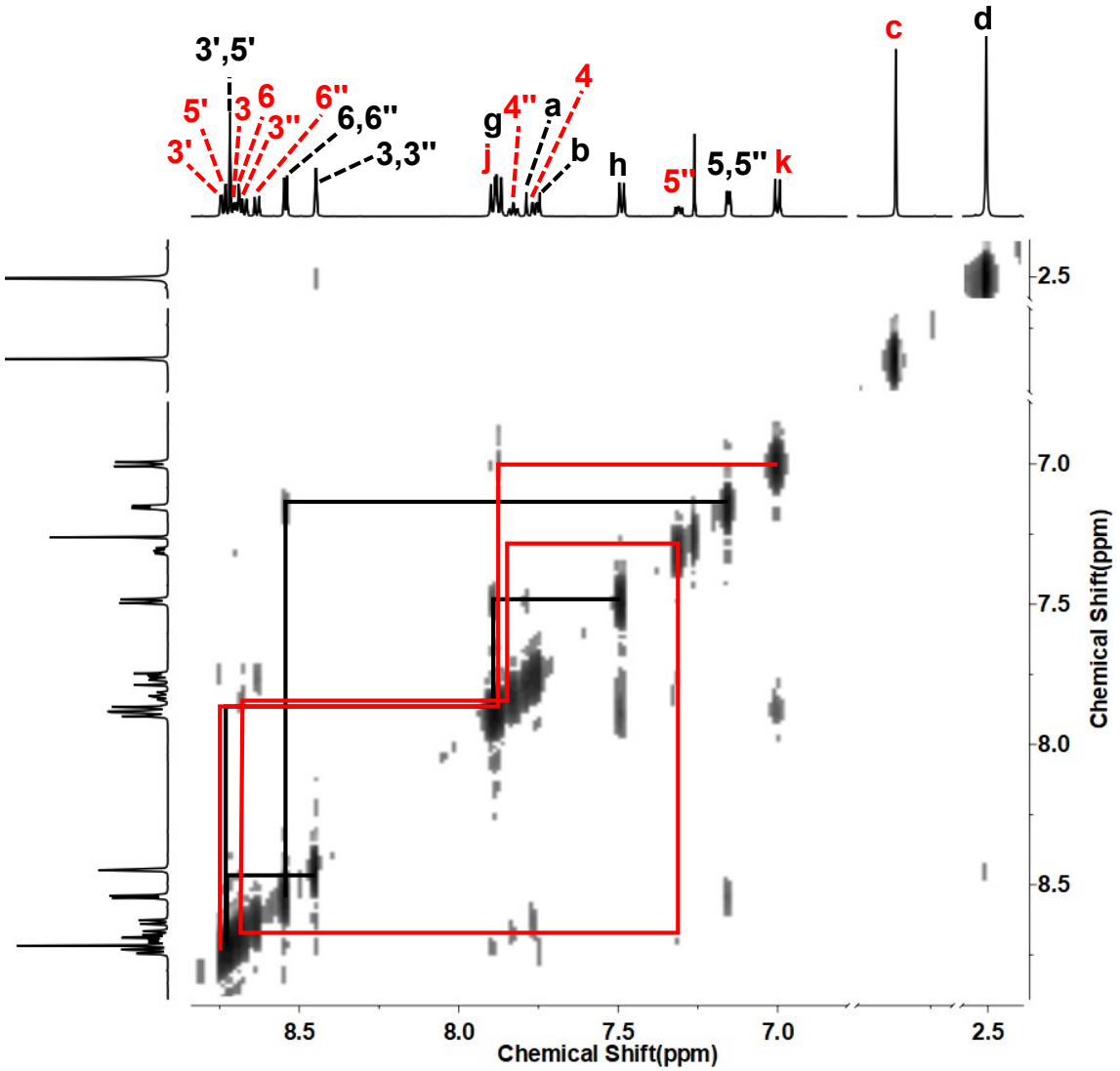

Figure S11: 2D NOESY spectrum (600 MHz, 298 K) of **L** in $CDCl_3$.

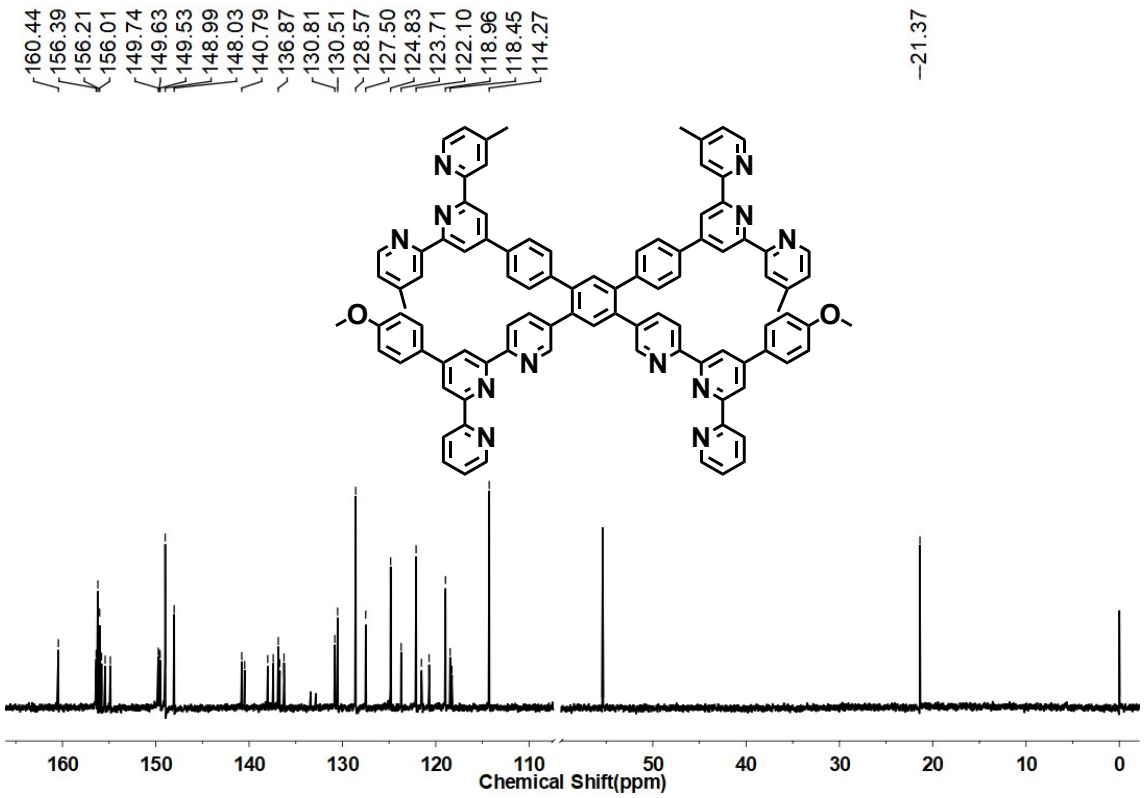

Figure S12: ^{13}C NMR spectrum (151 MHz, 298 K) of **L** in $CDCl_3$.

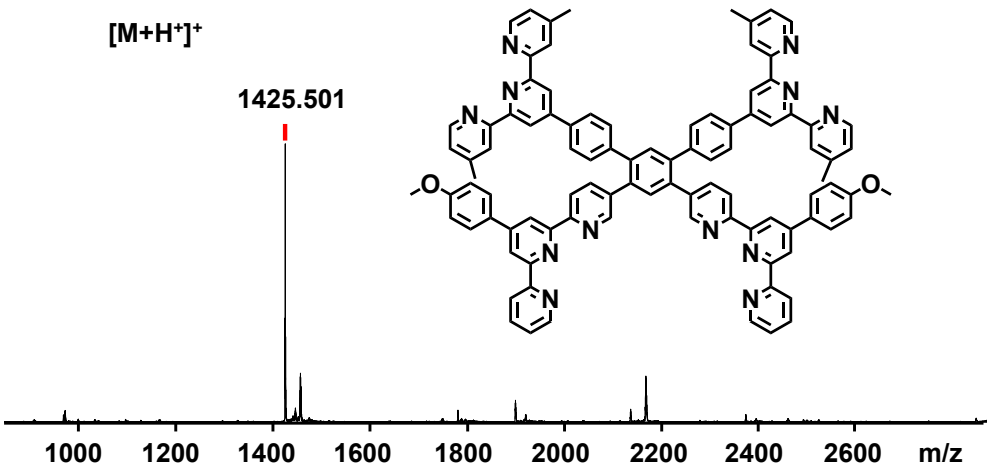

Figure S13: ESI-MS spectrum of **L**.

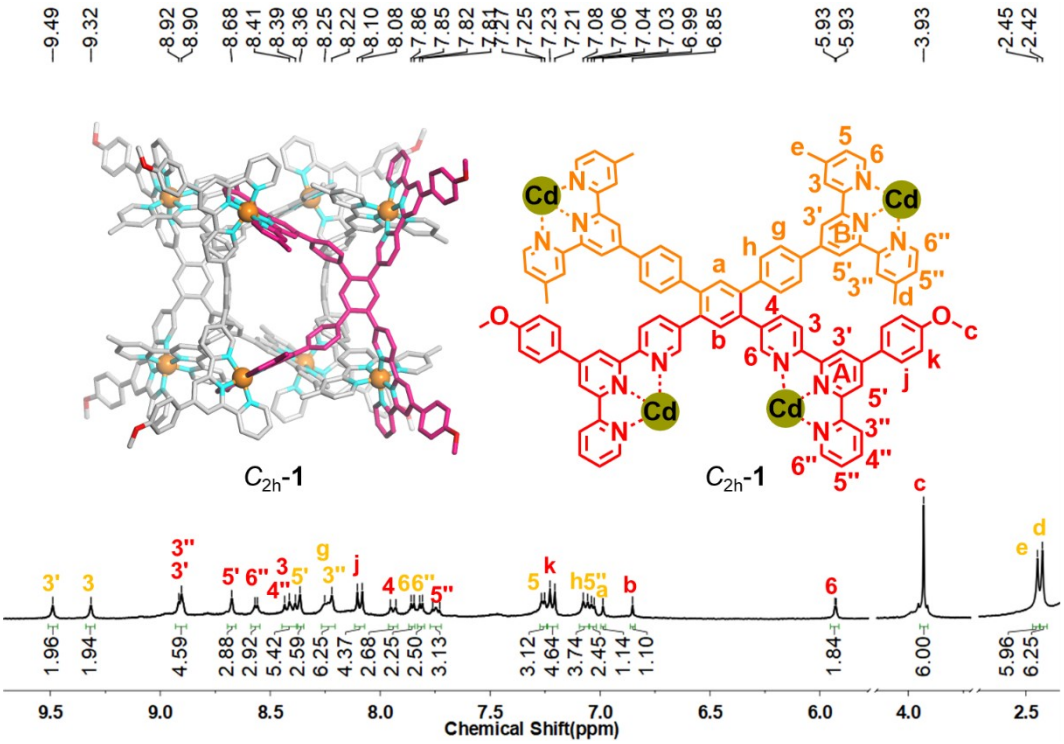

Figure S14: ^{1}H NMR spectrum (400 MHz, 298 K) of metallo-cube C_{2h}-**1** in CD_3CN.

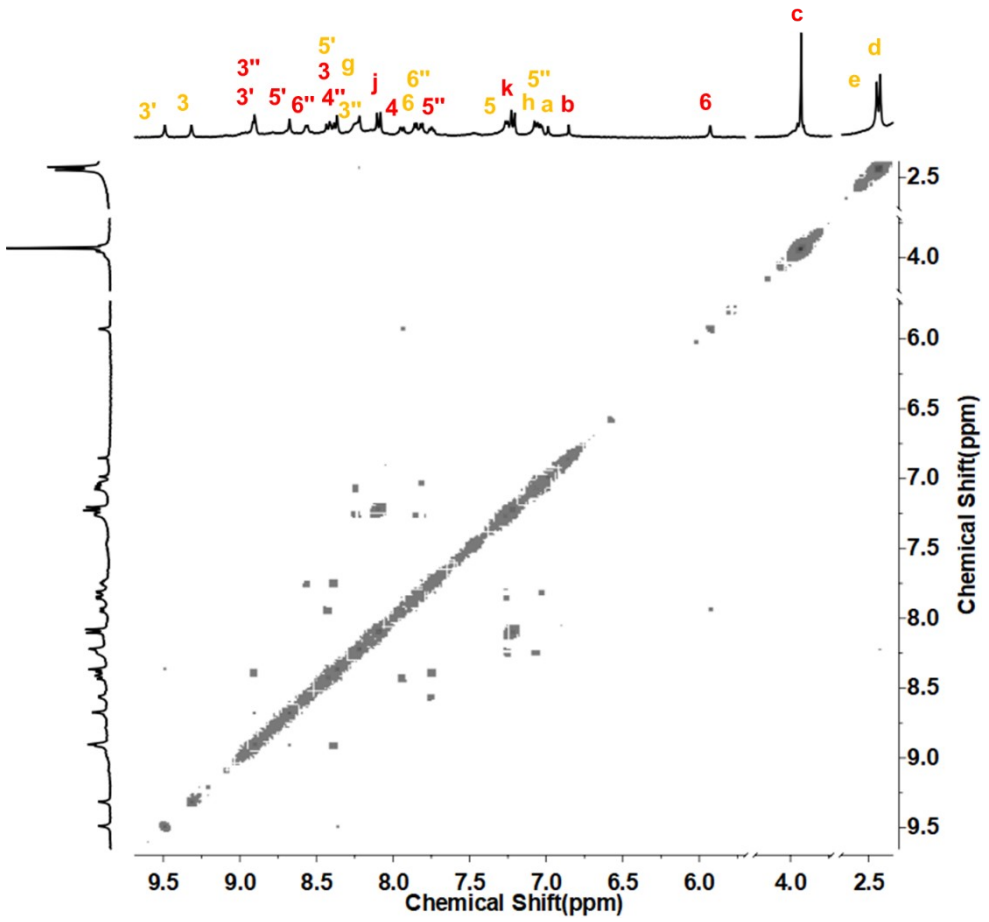

Figure S15: 2D COSY spectrum (400 MHz, 298 K) of metallo-cube C_{2h}-**1** in CD_3CN.

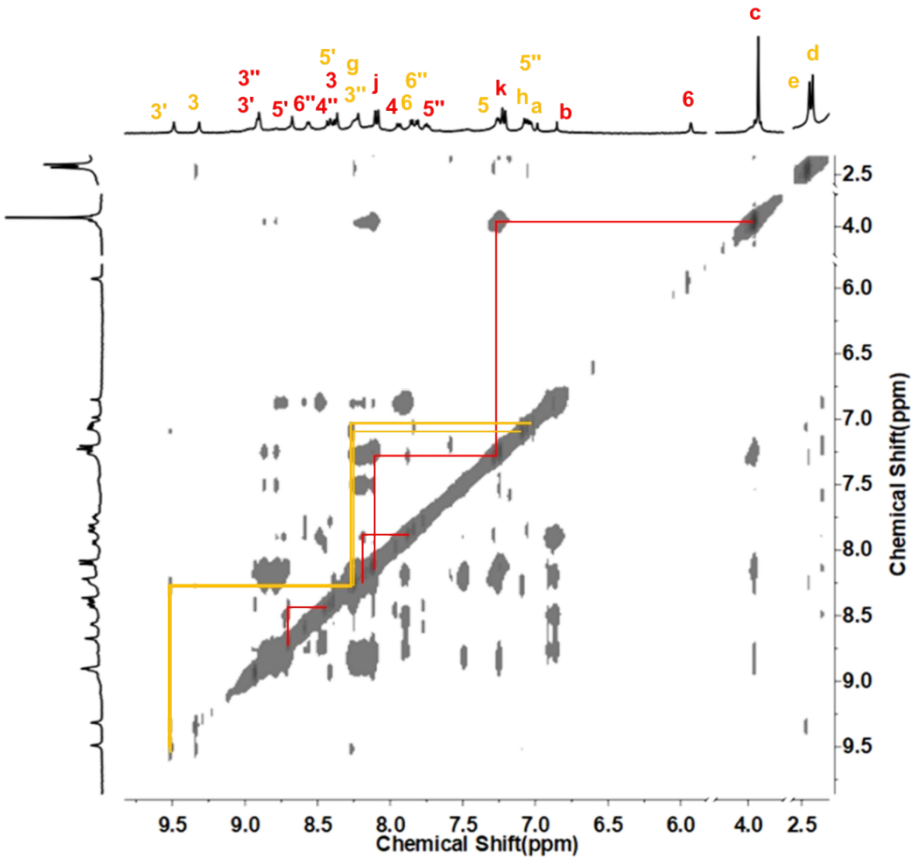

Figure S16: 2D NOESY spectrum (400 MHz, 298 K) of metallo-cube C_{2h}-**1** in CD_3CN.

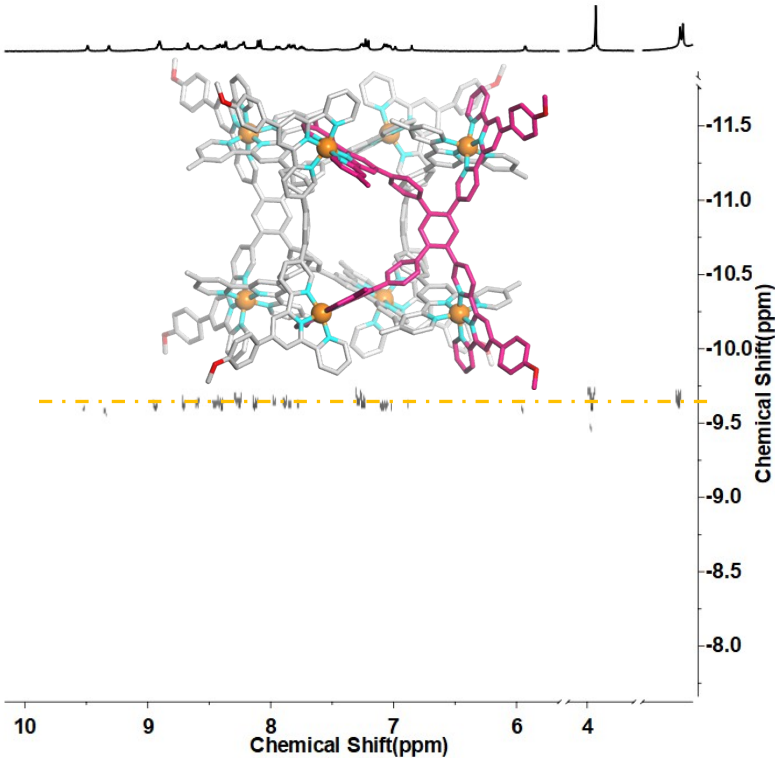

Figure S17: 2D DOSY spectrum (500 MHz, 298 K) of metallo-cube C_{2h}-**1** in CD_3CN.

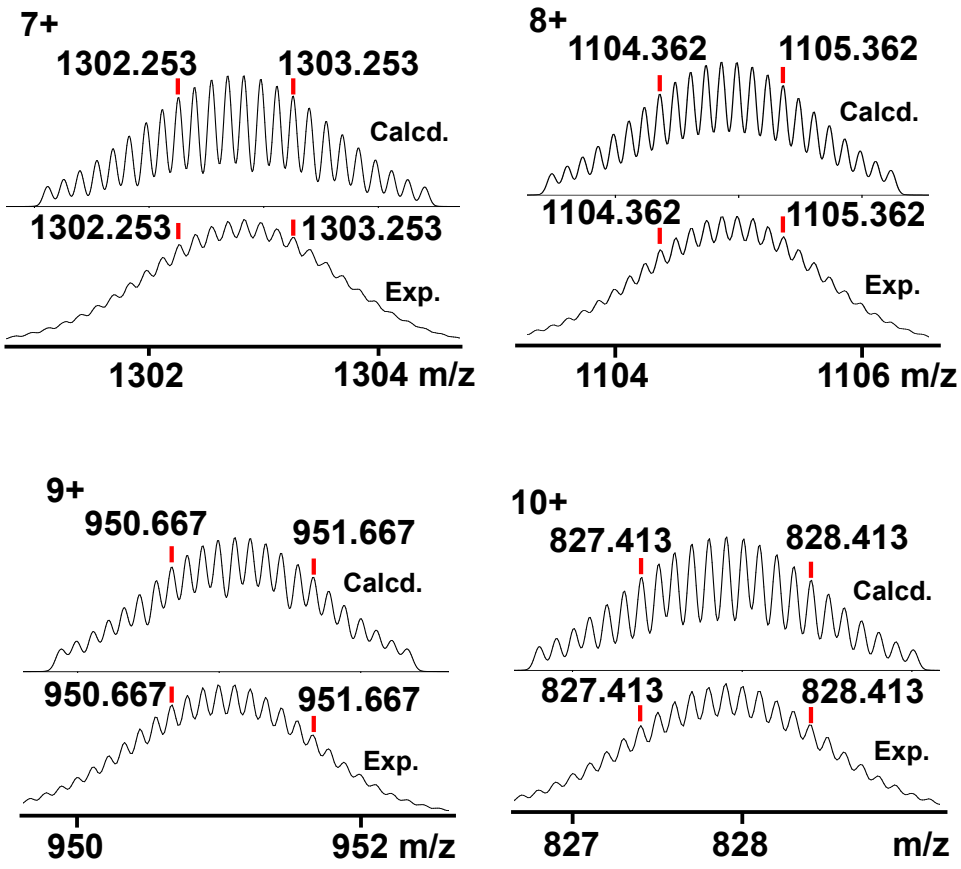

Figure S18: Isotope patterns spectrum of metallo-cube C_{2h}-**1** (NTf_2^- as counterion).

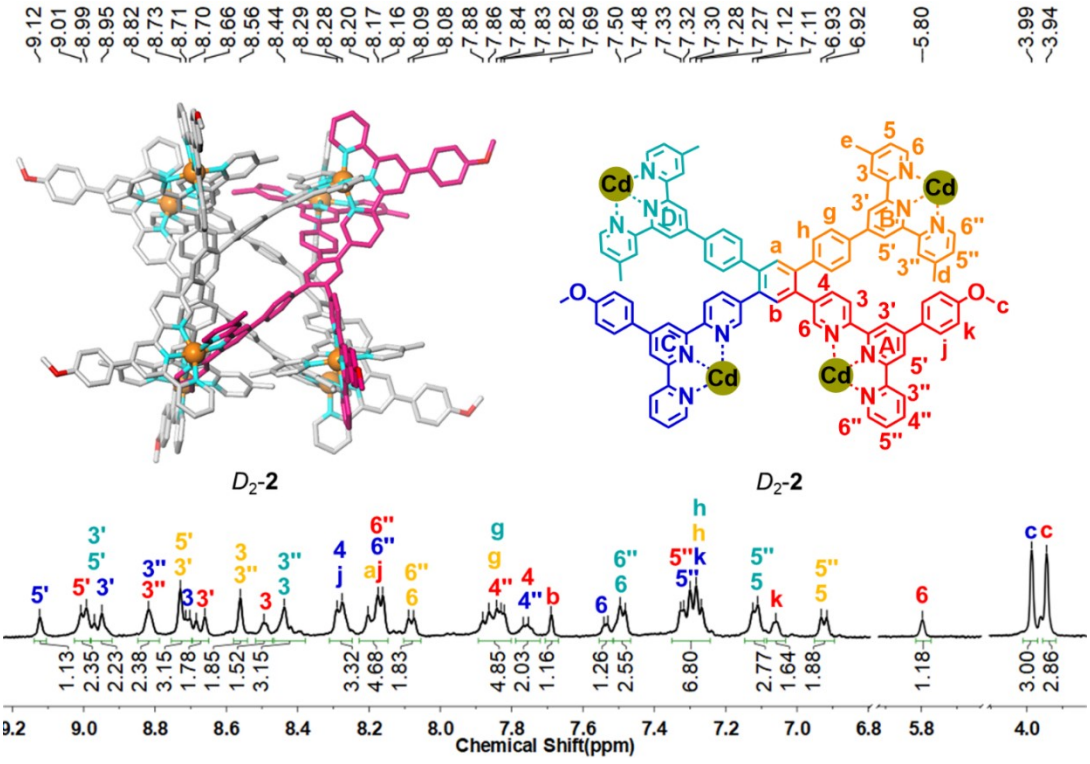

Figure S19: ^{1}H NMR spectrum (400 MHz, 298 K) of metallo-cube D_2-**2** in CD_3CN.

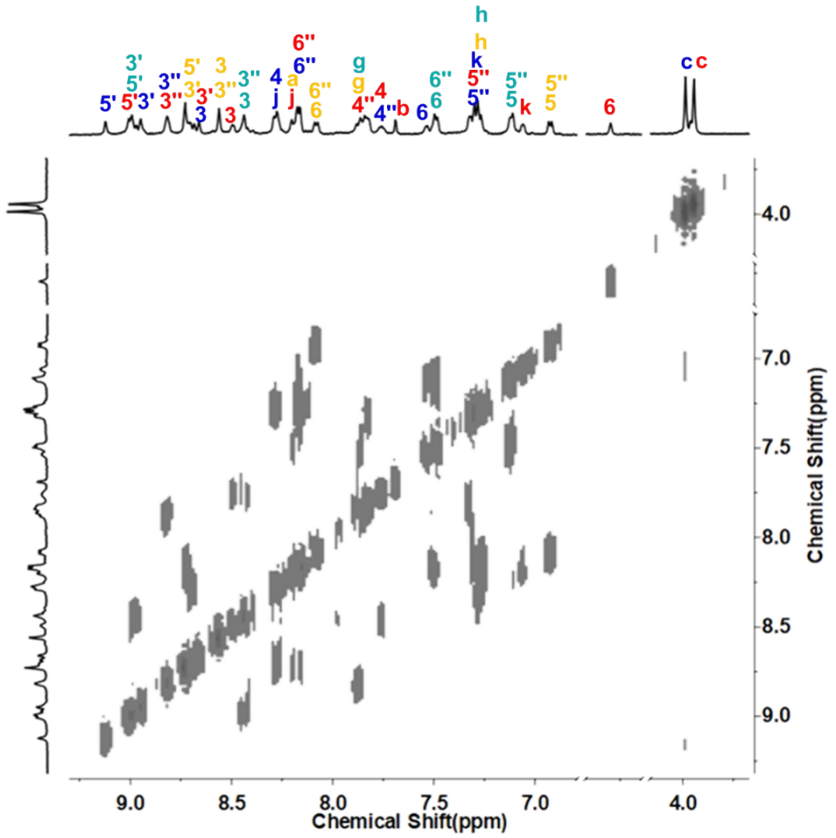

Figure S20: 2D COSY spectrum (400 MHz, 298 K) of metallo-cube D_2-**2** in CD_3CN.

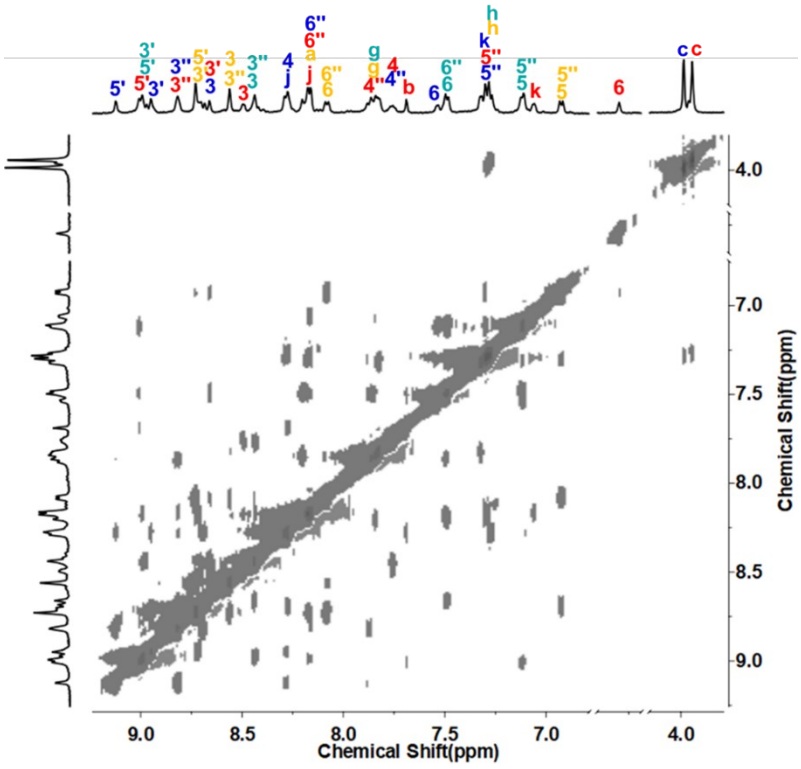

Figure S21: 2D NOESY spectrum (400 MHz, 298 K) of metallo-cube D_2-**2** in CD_3CN.

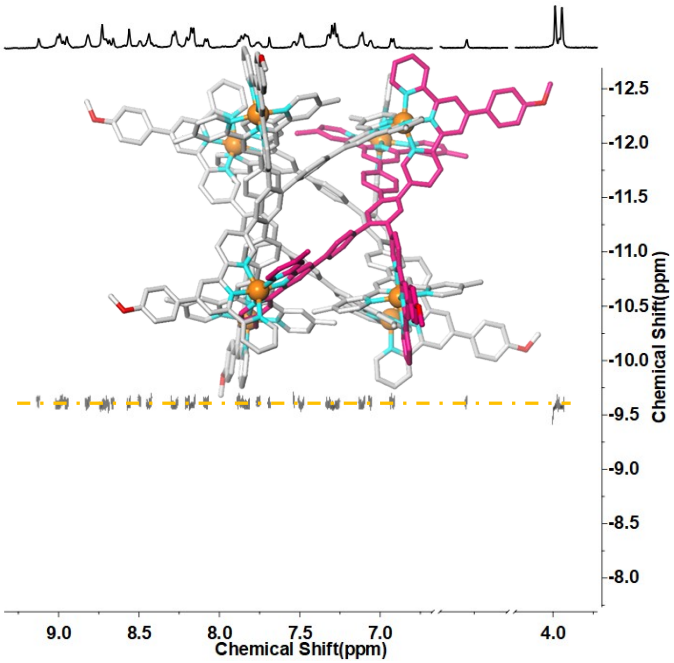

Figure S22: 2D DOSY spectrum (500 MHz, 298 K) of metallo-cube D_2-**2** in CD_3CN.

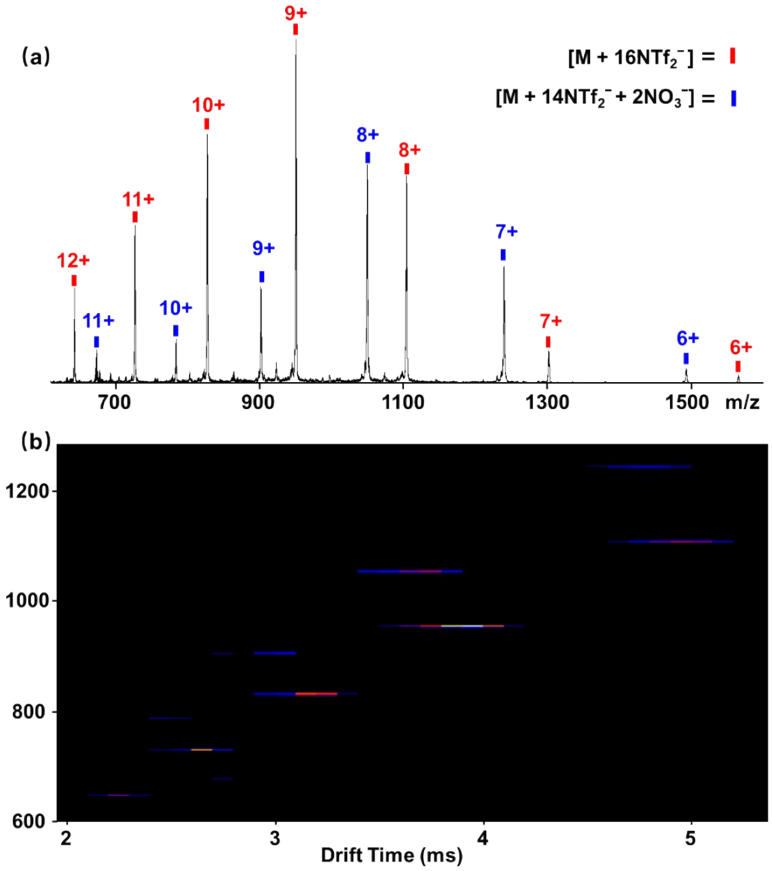

Figure S23: (a) ESI-MS spectrum and (b) ESI-TWIM-MS plot of metallo-cube D_2-**2** (NTf_2^- and NO_3^- as counterion).

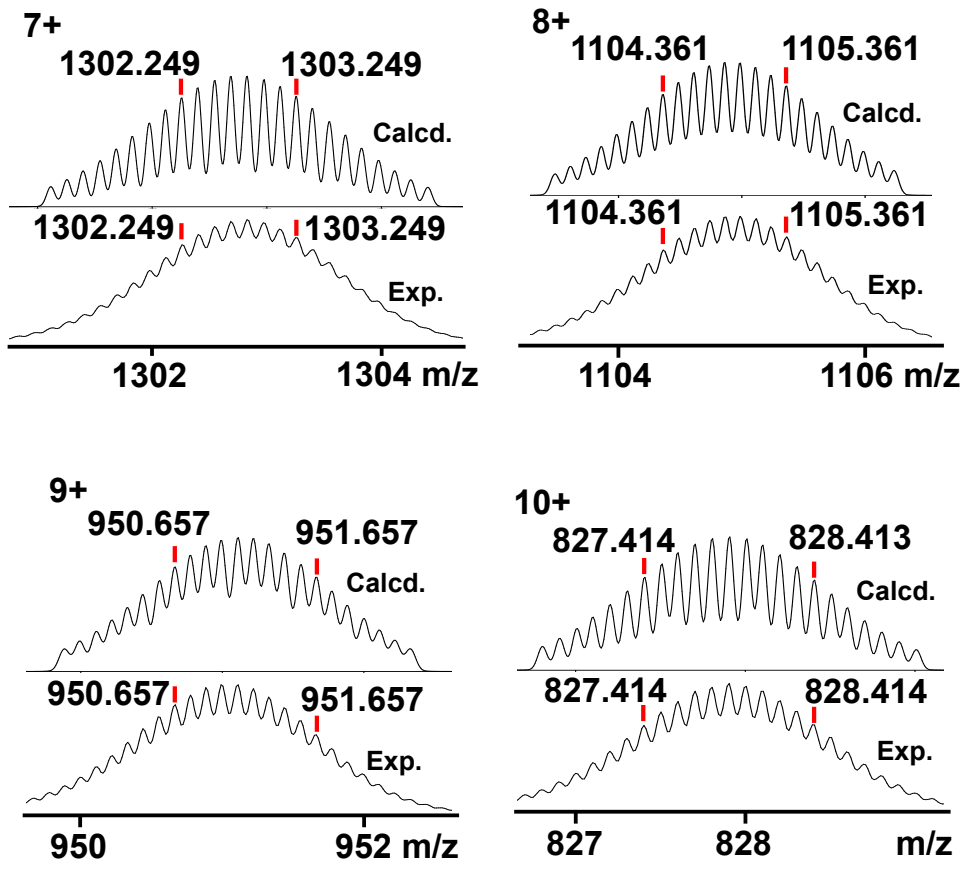

Figure S24: Isotope patterns spectrum of metallo-cube D_2-**2** (NTf_2^- as counterion).

4. Host-guest complexation

4.1 neutral guests with no encapsulation

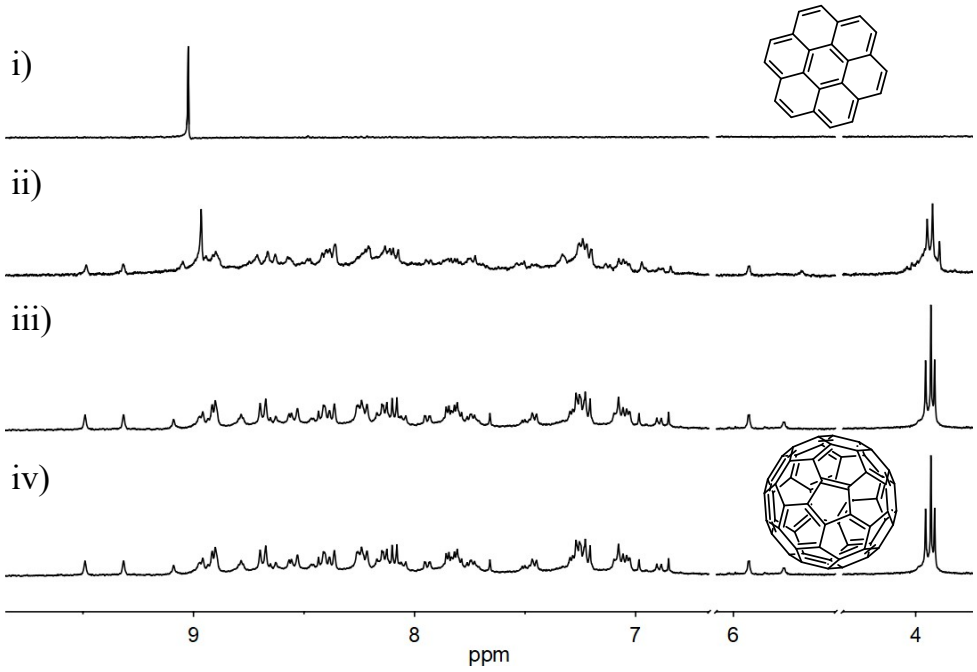

Figure S25: The comparison of ^{1}H NMR spectra (500 MHz, 298 K, CD_3CN-d_3) of i) coronene (CO R); ii) COR + (C_{2h}-**1** + D_2-**2**); iii) C_{2h}-**1** + D_2-**2**; iv) C_{60} + (C_{2h}-**1** + D_2-**2**). C_{60} and COR cannot be enc apsulated by C_{2h}-**1** + D_2-**2**.

4.2 anionic guests can be encapsulated by host but don't cause any equilibrium shift between two conformers.

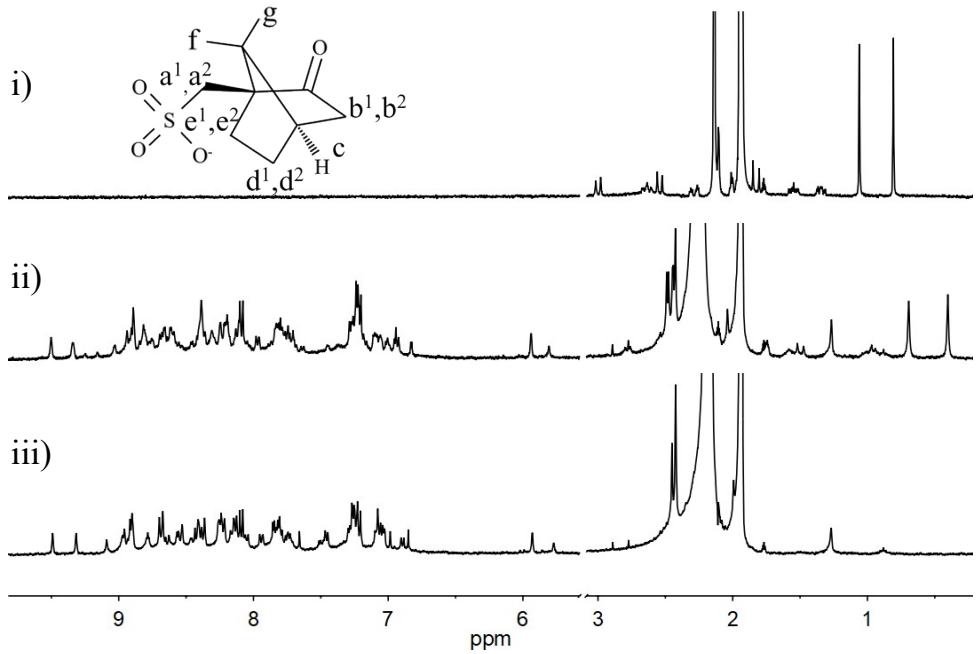

Figure S26: The comparison of full ^{1}H NMR spectra (500 MHz, 298 K, CD_3CN-d_3) of i) *D*-sodium

camphor sulfonate; ii) *D*-sodium camphor sulfonate + (C_{2h}-**1** + D_2-**2**); iii) C_{2h}-**1**+ D_2-**2**. *D*-sodium camp hor sulfonate can be encapsulated by C_{2h}-**1**+ D_2-**2**.

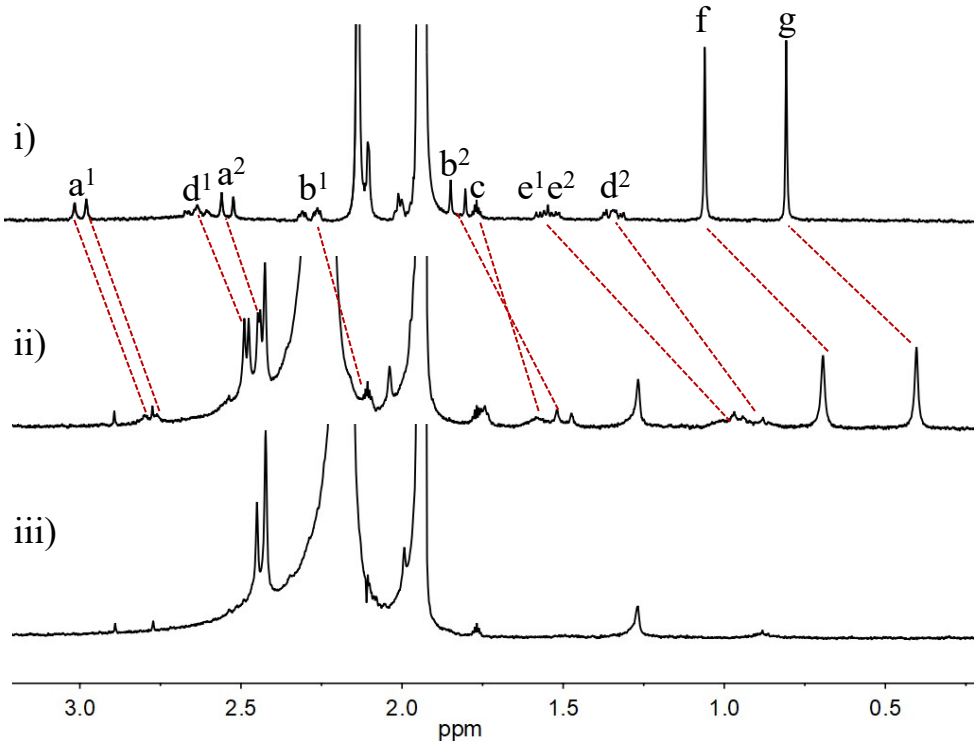

Figure S27: The comparison of enlarged ^{1}H NMR spectra (500 MHz, 298 K, CD_3CN-d_3) of i) *D*-sod ium camphor sulfonate; ii) *D*-sodium camphor sulfonate + (C_{2h}-**1** + D_2-**2**); iii) C_{2h}-**1**+ D_2-**2**. *D*-sodium camphor sulfonate can be encapsulated by C_{2h}-**1** + D_2-**2**.

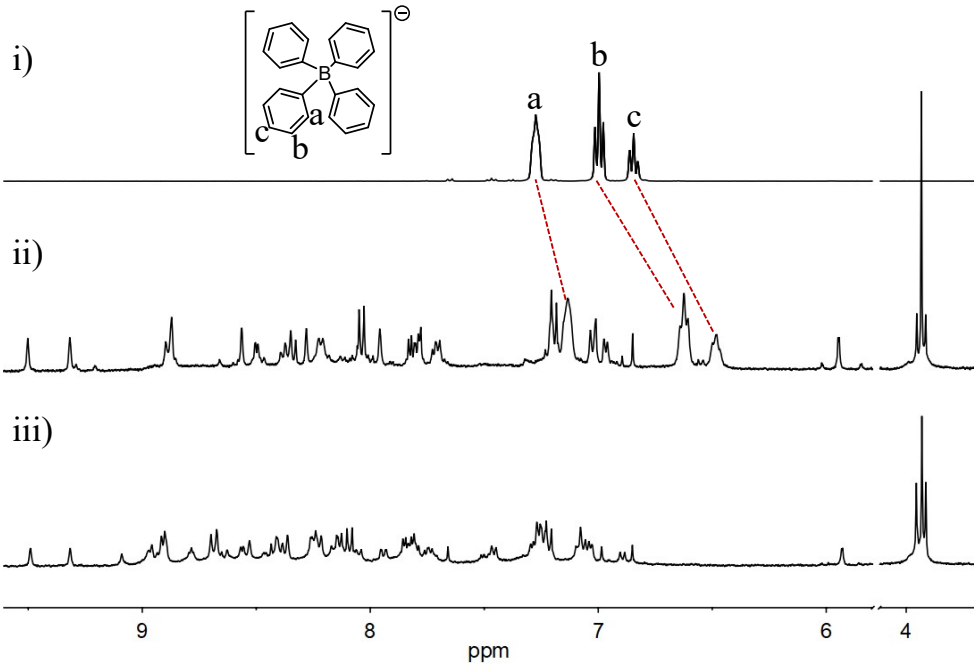

Figure S28: The comparison of ^{1}H NMR spectra (500 MHz, 298 K, CD_3CN-d_3) of i) tetra-n-butylamm

onium tetraphenylborate; ii) tetra-n-butylammonium tetraphenylborate + (C_{2h}-**1** + D_2-**2**); iii) C_{2h}-**1**+ D_2 -**2**. Tetra-n-butylammonium tetraphenylborate can be encapsulated by C_{2h}-**1**+ D_2-**2**.

4.3 anionic guest can be encapsulated and causes equilibrium shift between the two conformers.

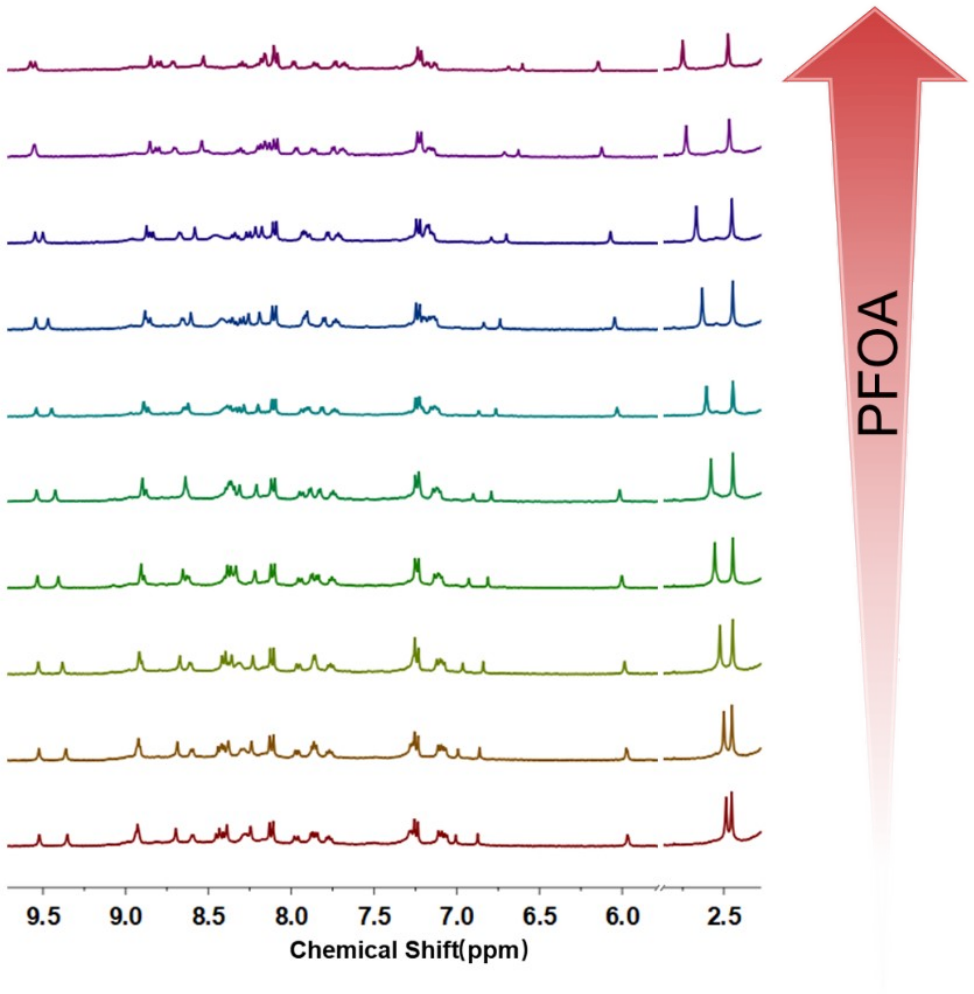

Figure S29: ^{1}H NMR titration with the continuous addition of sodium perfluorooctanoate into the so lution of metallo-cage C_{2h}-**1** (sodium perfluorooctanoate concentration gradually increasing from bot tom to top).

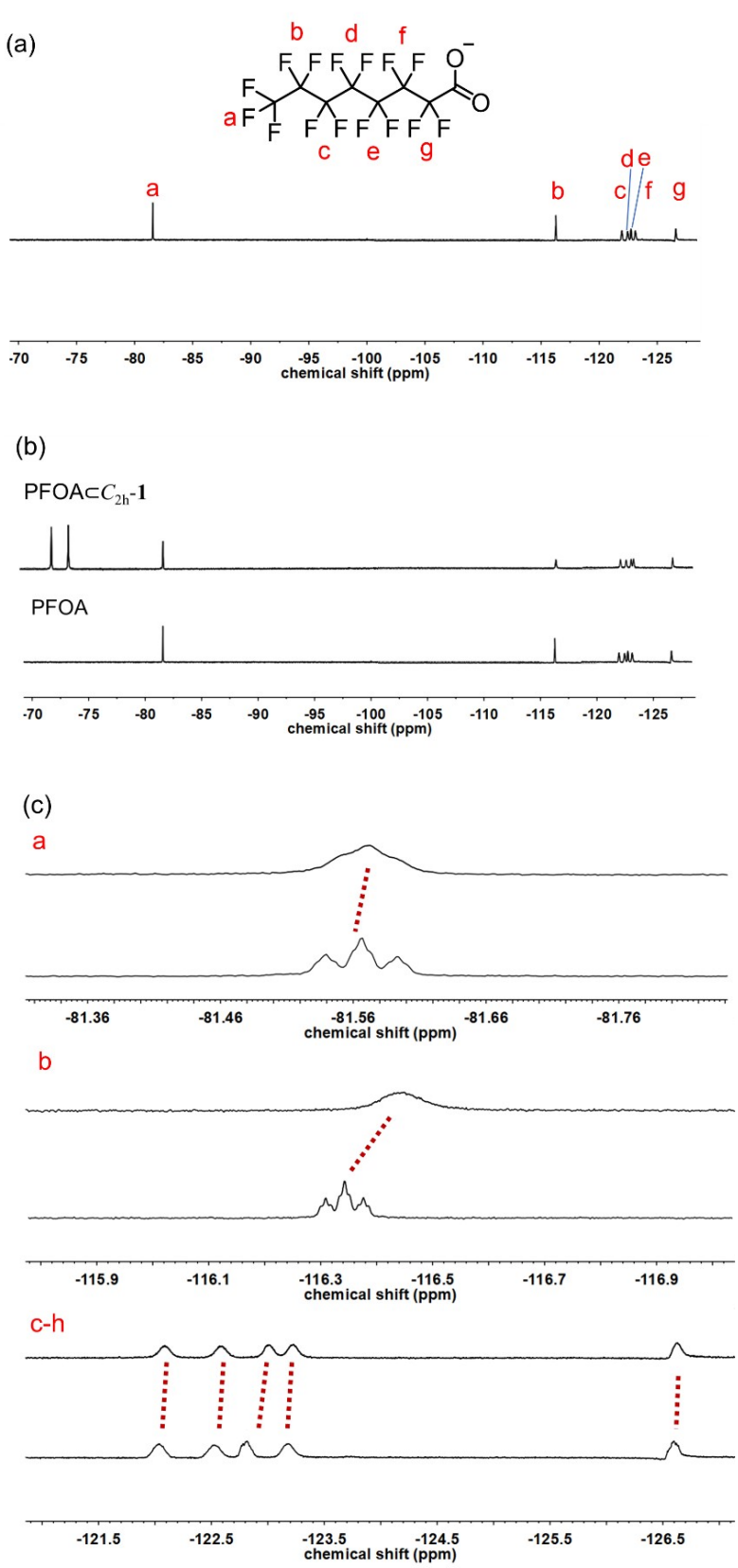

Figure S30: (a) ^{19}F NMR (500 MHz, CD_3CN, 298 K) spectra of PFOA; (b) ^{19}F NMR (500 MHz, CD_3CN, 298 K) spectra of the conformer C_{2h}-**1** and PFOA⊂ C_{2h}-**1**; (c) Partial ^{19}F NMR (500 MHz, CD_3CN, 298 K) spectra of (b).

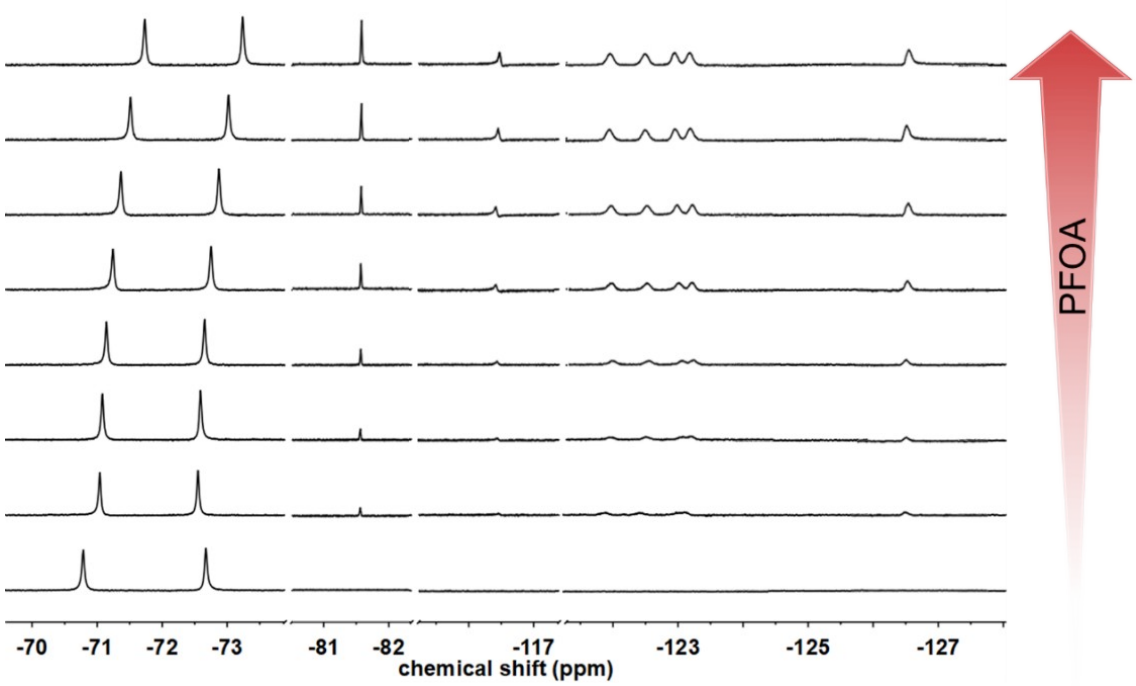

Figure S31: ^{19}F NMR (500 MHz, CD_3CN, 298 K) titration with the continuous addition of sodium perfluorooctanoate into the solution of metallo-cage C_{2h}-**1** (sodium perfluorooctanoate concentration gradually increasing from bottom to top).

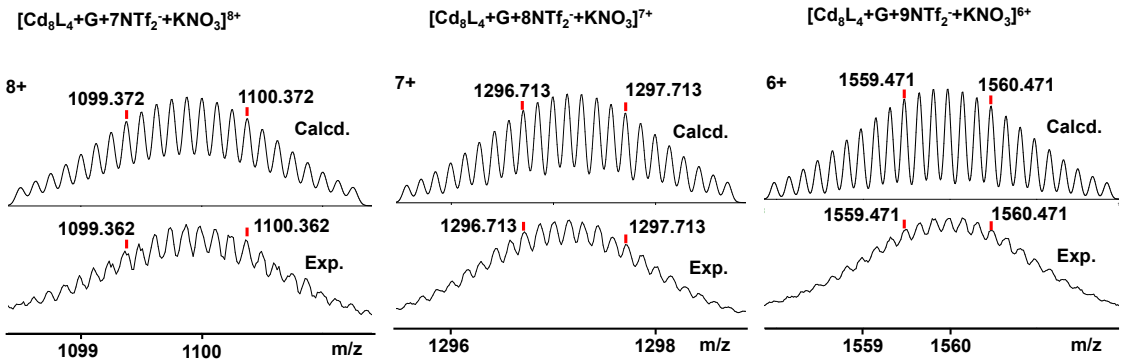

Figure S32: The isotopic patterns of three charge states (8+, 7+, 6+) in the host-guest complex PFOA⊂ C_{2h}-**1**.

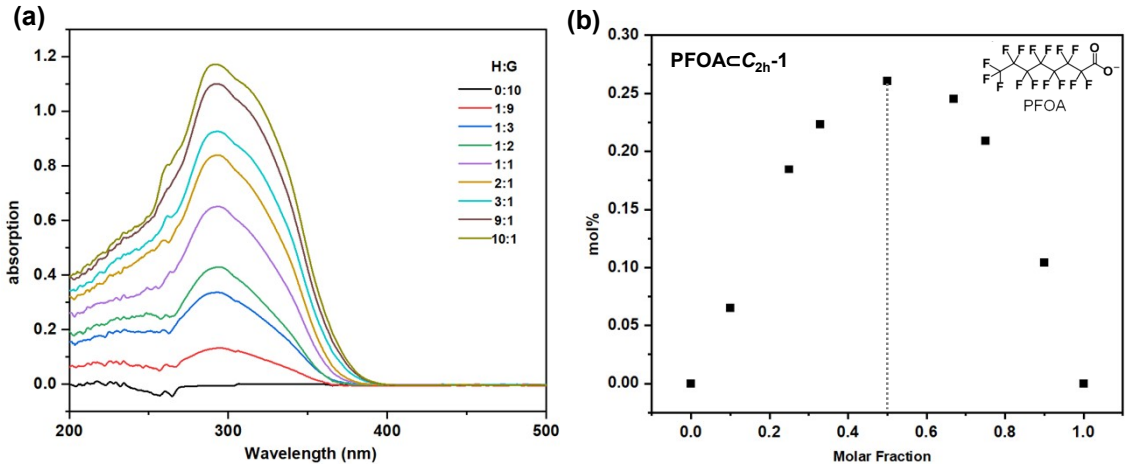

Figure S33: (a) UV-vis absorption of metallacage C_{2h}-**1** with PFOA in different molar ratios ([C_{2h}-**1**]+[PFOA]=6*10^{-6} mol/L); (b) Job's plot of the PFOA⊂C_{2h}-**1** in CH_3CN, showing a 1:1 stoichiometry.

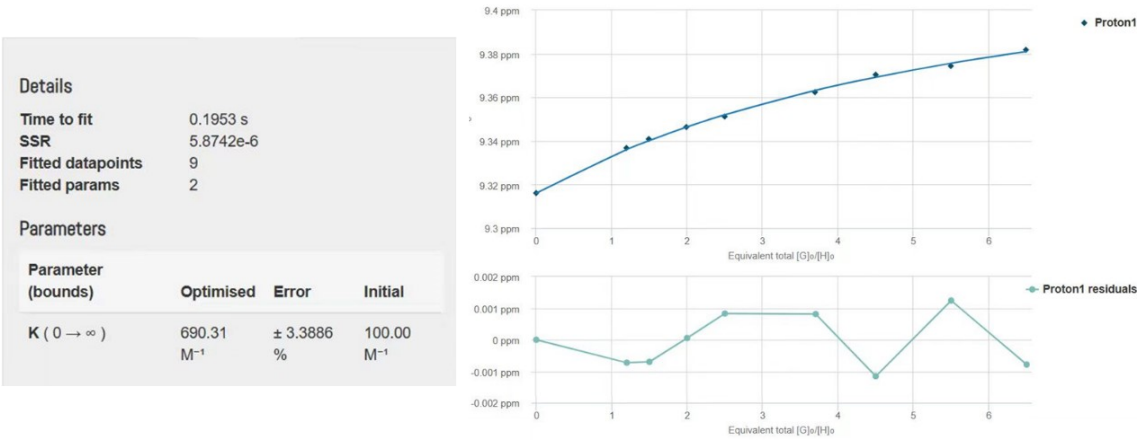

Figure S34: Binding isotherms (1:1 system) fitted to the chemical shift of proton signals vs. the equivalents of PFOA added to determine the binding affinity (top); and the residual plot from the fit (bottom).

5. Single-crystal X-ray diffraction (XRD)

The single crystals were obtained by slowly diffusing the vapor of isopropyl ether into complexes in acetonitrile for over one month.

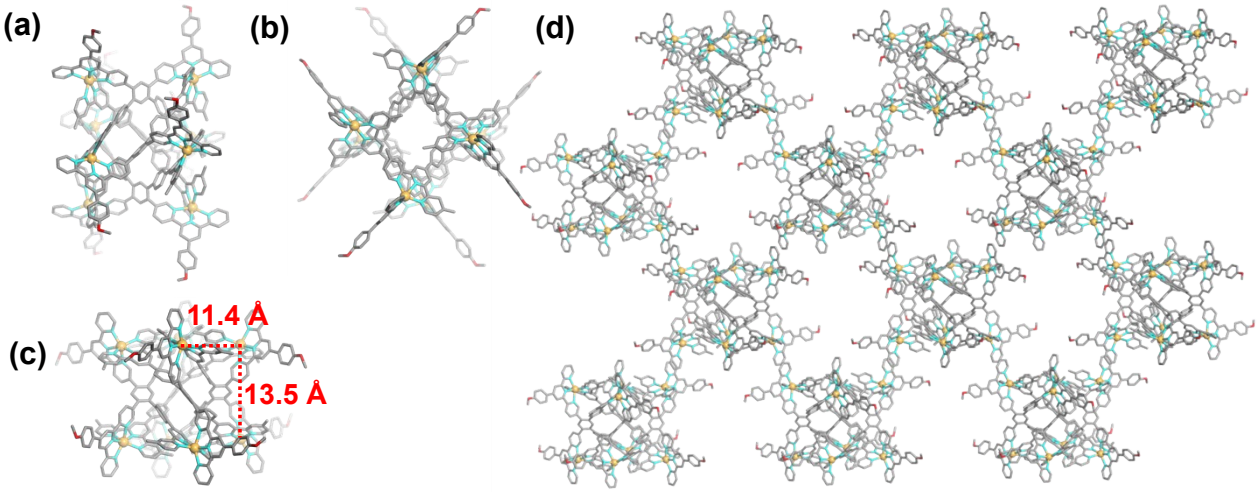

Figure S35: (a) The side view, (b) top view and (c) front view of crystal structure of metallo-cage D_2-**2**, (d) crystal packing model of metallo-cage D_2-**2**.

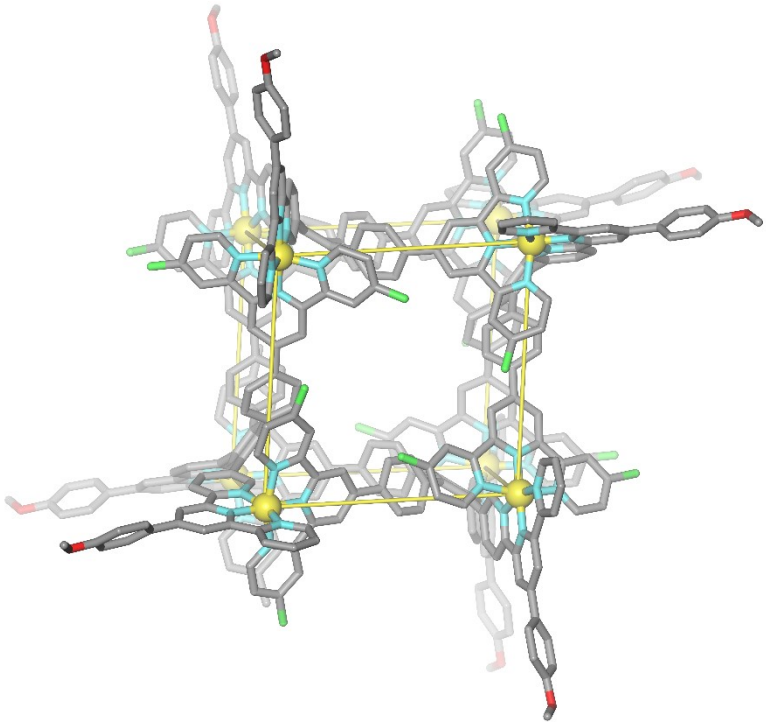

Figure S36: The methyl groups of part B (green marked) blocked the pore of C_{2h}-**1.**

Table S1. Crystal data and structure refinement for metallo-cube D_2-**2.**

Identification code	D_2-**2**
Empirical formula	$C_{416}Cd_8F_{96}N_{64}O_{72}S_{32}$
Formula weight	11076.20
Temperature/K	101.0
Crystal system	orthorhombic
Space group	Ccce
a/Å	28.333(3)
b/Å	43.635(4)
c/Å	40.669(4)
α/°	90
β/°	90
γ/°	90
Volume/Å^3	50280(9)
Z	8
ρ_{calc}g/cm^3	0.872
μ/mm^{-1}	2.035
F(000)	13512.0
Radiation	GaKα(λ = 1.34139)
2Θ range for data collection/°	3.746 to 68.288
Index ranges	$-23 \le h \le 23$, $-36 \le k \le 36$, $-33 \le l \le 33$
Reflections collected	127722
Independent reflections	7630 [R_{int} = 0.0839，R_{sigma} = 0.0416]
Data/restraints/parameters	7630/936/921
Goodness-of-fit on F^2	1.791
Final R indexes [I>=2σ (I)]	R_1 = 0.1328, wR_2 = 0.3859
Final R indexes [all data]	R_1 = 0.1563, wR_2 = 0.4148
Largest diff. peak/hole / e Å^{-3}	1.61/-0.53

6. Volume Calculations

In order to determine the available void spaces of C_{2h}-**1**, D_2-**2**, VOIDOO calculations based on the simulated energy optimal structure (for C_{2h}-**1**) and crystal structures (for D_2-**2**) were performed.[S3] A virtual probe with a radius of 1.4 Å (set by default, water-sized) was employed, and the standard parameters tabulated below were used.

Maximum number of volume-refinement cycles: 30

Minimum size of secondary grid: 3

Grid for plot files: 0.1

Primary grid spacing: 0.1

Plot grid spacing: 0.1

The cavity volumes were calculated to be 1263 and 867 Å^3 for C_{2h}-**1**, D_2-**2**, respectively.

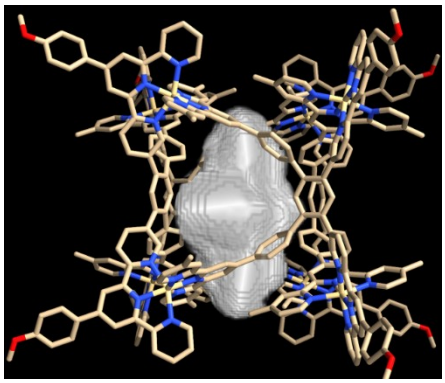

Figure S37: VOIDOO calculated void space within the crystal structure of C_{2h}-**1**. The volume is calculated to be 1263 Å^3.

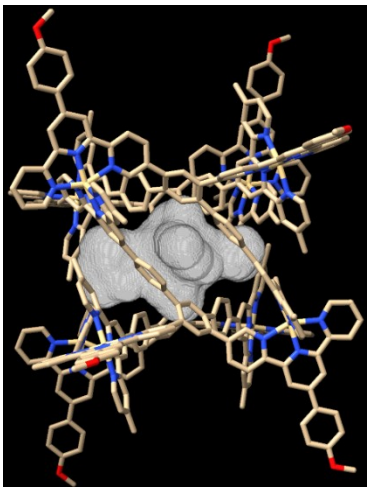

Figure S38: VOIDOO calculated void space within the crystal structure of D_2-**2**. The volume is calculated to be 867 Å^3.

7. Calculation

Molecular level understanding on the kind of interaction of the host with one conformer while the other conformer having less interaction with the guest has been checked. As shown in Figure 40, part of the fluorine atoms in guest PFOA interacted with hydrogen atoms in conformer D_2-**2** through CH…F hydrogen bonds with about 2.7-3.4 Å distance (about 6 CH…F hydrogen bonds), indicating low bond energy. In terms of PFOA⊂C_{2h}-**1** host-guest complex, all of the fluorine atoms in guest PFOA interacted with hydrogen atoms in conformer C_{2h}-**1** through CH…F hydrogen bonds with about 2.1-3.1 Å distance (about 11 CH…F hydrogen bonds), showing strong bonding energy (Figure 41). So, the difference of hydrogen bonds between hosts and guest PFOA is the driving force for encapsulation of the guest in conformer C_{2h}-**1** rather than conformer D_2-**2**.

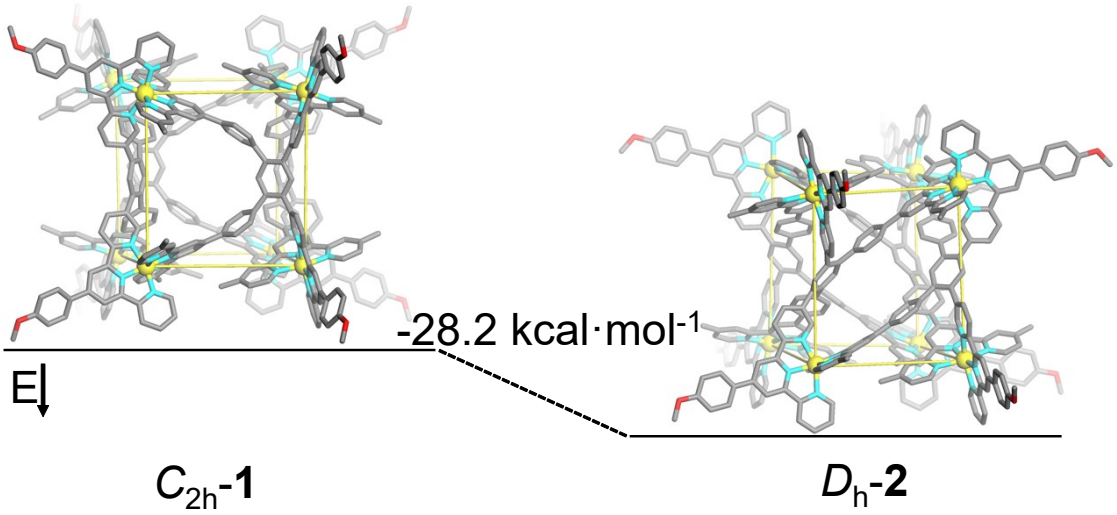

Figure S39: The energy-minimized structure of C_{2h}-**1**, single-crystal structure of D_2-**2**. The energy difference between two structures is presented.

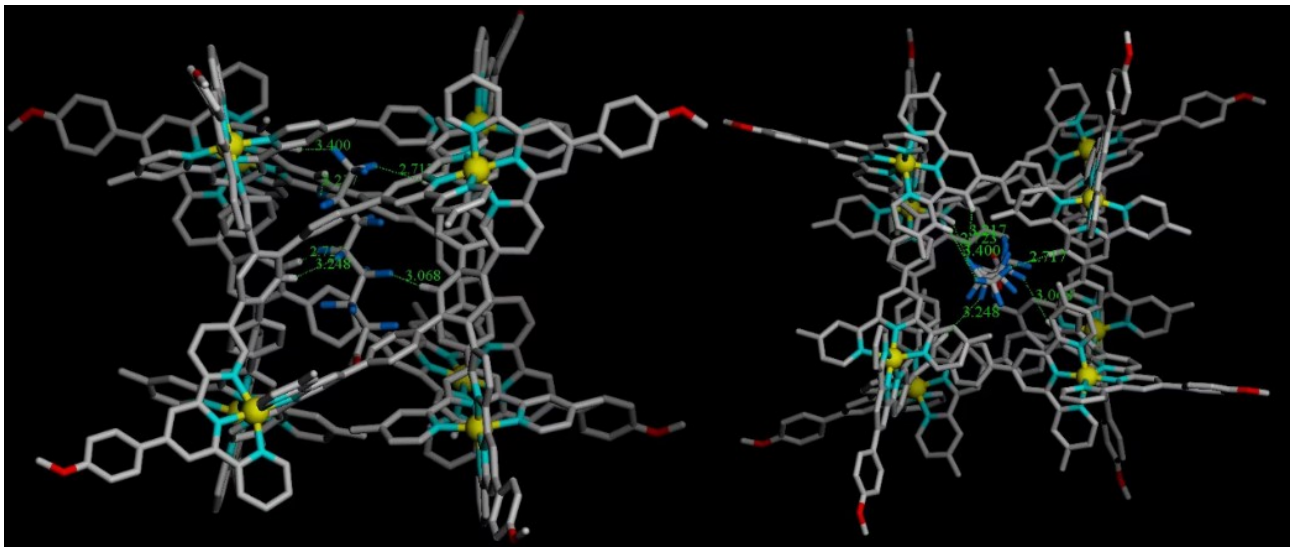

Figure S40: CH…F hydrogen bonds in PFOA⊂D_2-**2**.

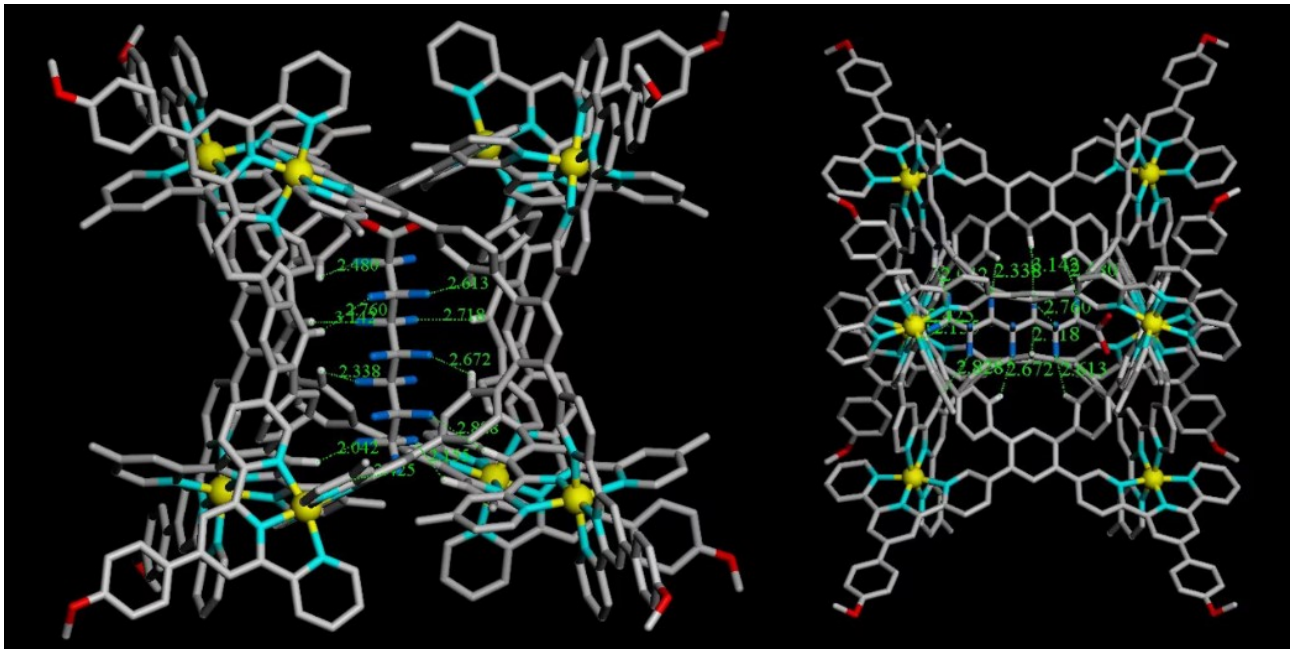

Figure S41: CH…F hydrogen bonds in PFOA⊂C_{2h}-**1**.

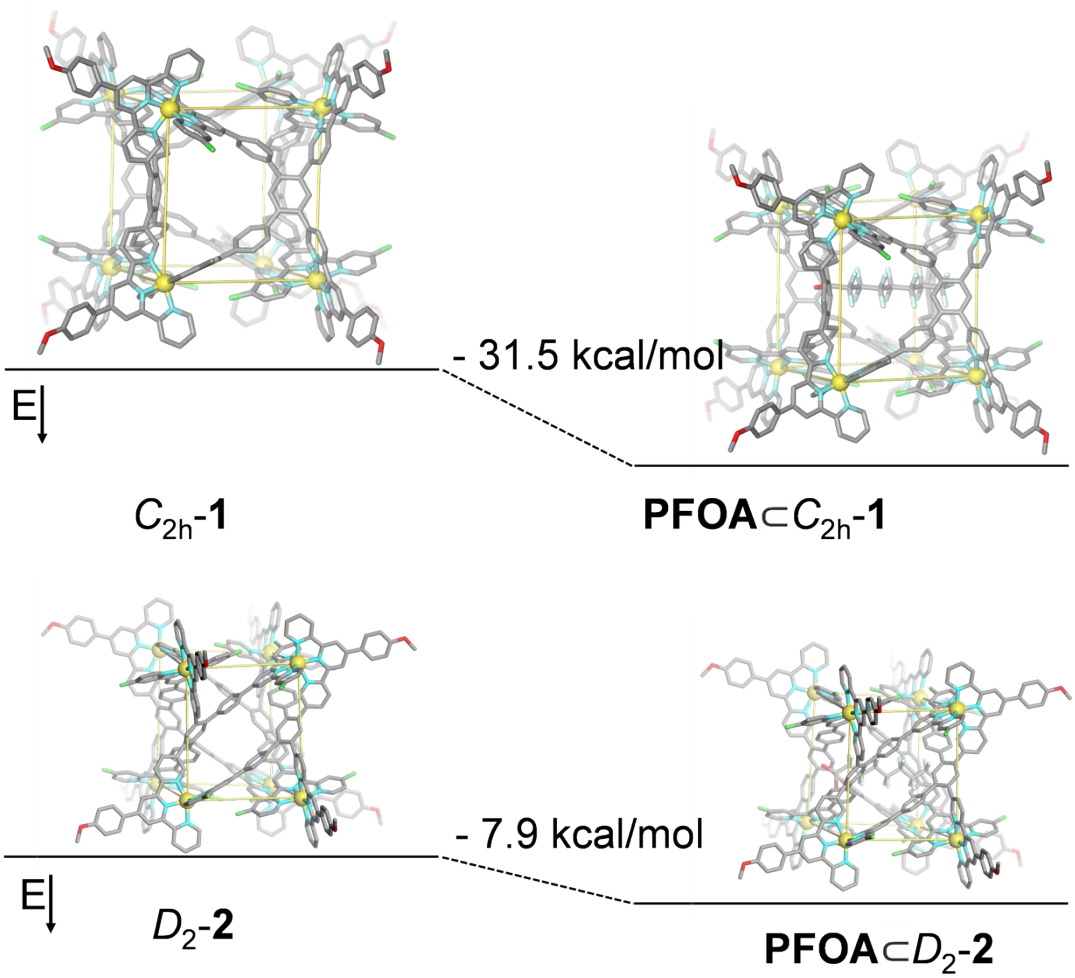

Figure S42: The binding energies of host-guest complex PFOA⊂C_{2h}-**1** and PFOA⊂D_2-**2**.

8. The NMR and MS spectra date of Zn_8L_4

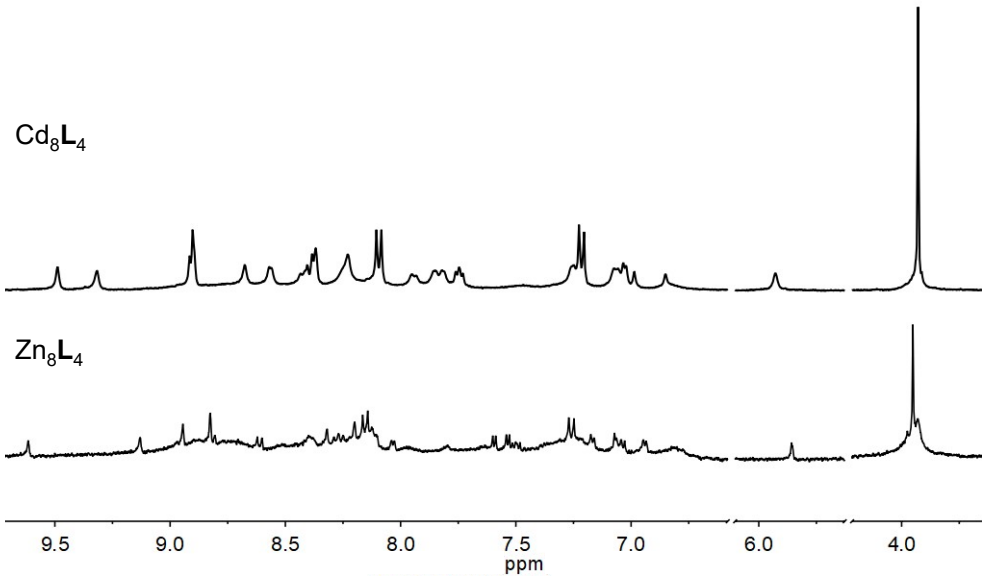

Figure S43: The comparison of ^{1}H NMR spectra of metallo-cage Cd_8L_4 and Zn_8L_4 (500 MHz, 298 K, CD_3CN-d_3).

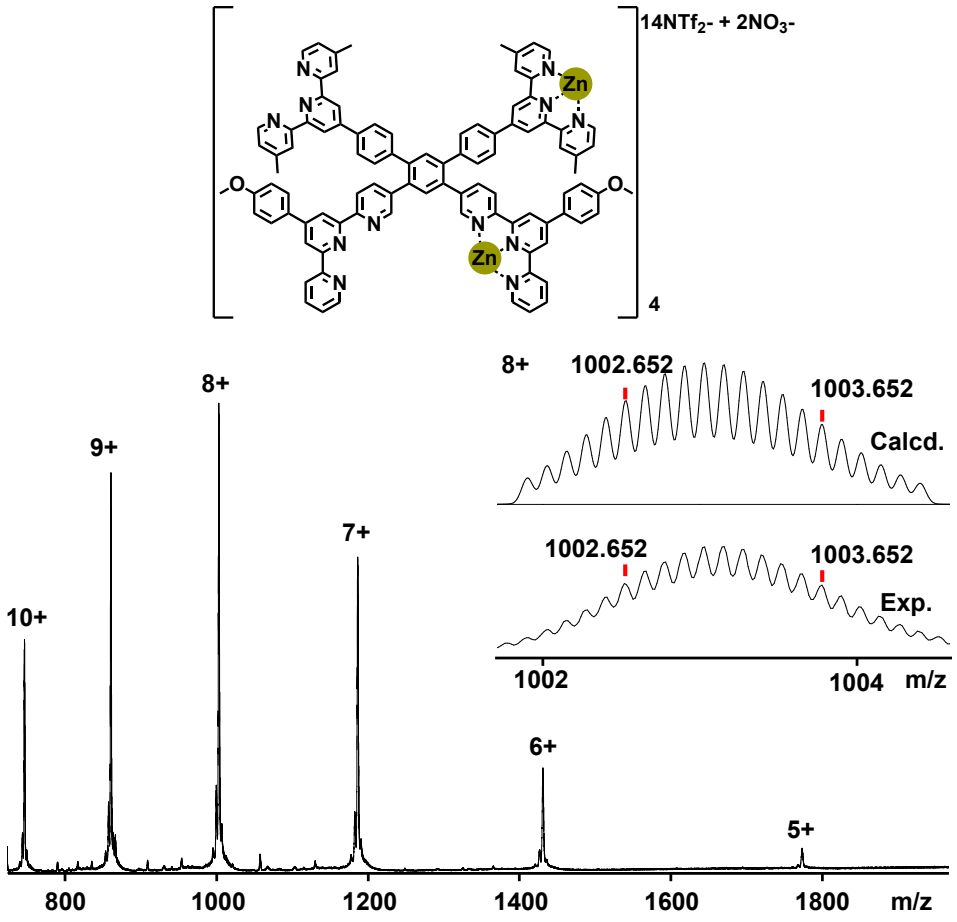

Figure S44: ESI-MS spectra of metallo-cage Zn_8L_4 with insert isotopic patter of charge state 8+.

9. References

S1. Y. Liu, Z. Jiang, Y. Guan, Q. Bai, Z. Zhang, Y. Li, H. Zhao, T.-Z. Xie, M. Wang, P. Wang and T. Wu, Halide ion directed templation effect of quadruple-stranded helicates, *Cell Rep. Phys. Sci.*, 2022, **3**, 101056.

S2. J. Wang, Z. Jiang, J.-F. Yin, H. Zhao, Q. Dong, K. Li, W. Zhong, D. Liu, J. Yuan, P. Yin, Y. Li, Y. Lin, M. Chen and P. Wang, Strain-Induced Heteromorphosis Multi-Cavity Cages: Tension-Driven Self-Expansion Strategy for Controllable Enhancement of Complexity in Supramolecular Assembly, *Angew. Chem. Int. Ed.*, 2024**, 63**, e202317674.

S3. C. Xu, Q. Lin, C. Shan, X. Han, H. Wang, H. Wang, W. Zhang, Z. Chen, C. Guo, Y. Xie, X. Yu, B. Song, H. Song, L. Wojtas and X. Li, Metallo-Supramolecular Octahedral Cages with Three Types of Chirality towards Spontaneous Resolution, *Angew. Chem. Int. Ed.*, 2022**, 61***,* e202203099.

S4. O. V. Dolomanov, L. J. Bourhis, R. J. Gildea, J. A. K. Howard and H. Puschmann, link to html 5 OLEX2: a complete structure solution, refinement and analysis program, *J. Appl. Cryst.* 2009, **42**, 339–341.

S5. G. M. Sheldrick, SHELXT – Integrated space-group and crystal-structure determination, *Acta Cryst. A*. 2015, **71**, 3–8.

S6. G. M. Sheldrick, Crystal structure refinement with SHELXL, *Acta Cryst. C*. 2015, **71**, 3–8.

S7. P. van der Sluis and A. L. Speck, BYPASS: an effective method for the refinement of crystal structures containing disordered solvent regions, *Acta Cryst*. *A*. 1990, **46**, 194−201.

S8. A. L. Spek, Single-crystal structure validation with the program PLATON, *J. Appl. Cryst.* 2003, **36**, 7-13.

S9: P. Pachfule, Y. Chen, S. C. Sahoo, J. Jiang, R. Banerjee, Structural Isomerism and Effect of Fluorination on Gas Adsorption in Copper-Tetrazolate Based Metal Organic Frameworks. *Chem. Mater.* 2011, **23**, 2908−2916.

S10. D. E. Coupry, M. A. Addicoat, T. Heine, Extension of the Universal Force Field for Metal–Organic Frameworks. *J. Chem. Theory Comput.* 2016, **12**, 5215−5225.